DEVELOPMENT AND EVALUATION OF TONGUE OPERATED ROBOTIC REHABILITATION PARADIGM FOR STROKE SURVIVORS WITH UPPER LIMB PARALYSIS

A Dissertation
Presented to
The Academic Faculty

by

Zhenxuan “James” Zhang

In Partial Fulfillment
of the Requirements for the Degree
Doctor of Philosophy in the
School of Electrical and Computer Engineering

Georgia Institute of Technology
August 2020

DEVELOPMENT AND EVALUATION OF TONGUE OPERATED ROBOTIC REHABILITATION PARADIGM FOR STROKE SURVIVORS WITH UPPER LIMB PARALYSIS

Approved by:

Dr. Boris I. Prilutsky, Advisor
School of Biological Science
Georgia Institute of Technology

Dr. Minoru "Shino" Shinohara
School of Biological Science
Georgia Institute of Technology

Dr. Patricio A. Vela
School of Electrical and Computer Engineering
Georgia Institute of Technology

Dr. Justin Romberg
School of Electrical and Computer Engineering
Georgia Institute of Technology

Dr. Andrew J. Butler
School of Health Professions
The University of Alabama at Birmingham

Date Approved: July 23rd, 2020

To my grandmother and others who are suffering from devastating conditions like stroke.

ACKNOWLEDGEMENTS

I want to express my sincere appreciate to my supervisor Dr. Boris I. Prilutsky. I have learned to pay attention to detail and conduct research with high intergrity standard. Moreover, he taught me to have a humble attitude when collaborating with others. I also want to thank Dr. Minoru Shinohara. Through our meetings and manuscript revisions, he taught me how to formulate research questions and design experiment like a scientist. I also want to thank my former supervisor Dr. Maysam Ghovanloo. He taught me that life has no short cut. One must work hard to achieve more. I am also thankful to Dr. Andrew Butler for his encouragement and advice. He inspires me to be more compasionate to others. I also want to thank Dr. Patricio Vela for his support especially in an emotional level. Specifically, he provided the positive environment for me to conduct research when I was in the transition period between advisors. I also want to thank all the other professors who has contributed to either my research or course work at Georgia Tech. Specially, I want to thank Dr. Justin Romberg and Dr. Rincon-Mora for giving some of my favorite lectures.

This thesis work would be difficult to complete without the generous financial support of various funding sources which include Marcus Foundation, National Science Foundation, National Institute of Health, and School of Electrical and Computer Engineering at Georgia Tech.

In addition, I want to thank my colleague from GT-Bionics, Biomechanics and Motor Control Lab, and other collaborators. It is wonderful to work with someone who are

also passionate about engineering, science, and healthcare. I also want to thank all the participants involved in this research.

Finally, I want to thank my family members for their support and guidance. In additiona, I also want to thank Mr. Matthew Fields for igniting my initial interests in biological science.

TABLE OF CONTENTS

ACKNOWLEDGEMENTS **iv**

LIST OF TABLES **viii**

LIST OF FIGURES **ix**

LIST OF SYMBOLS AND ABBREVIATIONS **xiii**

SUMMARY **xiv**

Chapter 1 Introduction **1**
1.1 Background and Motivation **1**
1.2 Specific Aims **5**
1.2.1 Specific Aim 1: Enhancement and evaluation of a tongue-operated wrist robotic rehabilitation system 5
1.2.2 Specific Aim 2: Design and evaluation of a tongue-operated upper limb rehabilitation system 5
1.2.3 Specific Aim 3: Analysis of arm reaching movement controlled by a tongue-operated exoskeleton system: Implications for stroke rehabilitation 6
1.2.4 Specific Aim 4: Analysis of brain excitability at the onset of wrist and tongue movement 6

Chapter 2 Enhancement and evaluation of a tongue-operated wrist robotic rehabilitation system **7**
2.1 Introduction **7**
2.2 System Description **8**
2.2.1 BLE Based eTDS Headset 9
2.2.2 TDS-HM Interface Design 10
2.2.3 TDS-HM Control Modes 11
2.2.4 Tasks and Graphic User Interface 12
2.3 Performance Evaluation **12**
2.4 Conclusion **15**

Chapter 3 Design and evaluation of a tongue-operated upper limb rehabilitation system 17
3.1 Introduction **17**
3.2 Methods **19**
3.2.1 System Description 19
3.2.2 Tasks 21
3.2.3 Control Modes 23
3.2.4 Experimental Protocol 24
3.3 Results **26**
1.1 Discussion and Conclusion **32**

Chapter 4 Analysis of arm reaching movement controlled by a tongue-operated exoskeleton system: Implications for stroke rehabilitation **35**
4.1 Introduction **35**
4.2 Methods **36**
4.3 Results **41**
4.4 Conclusion **42**

Chapter 5 Analysis of brain excitability at the onset of wrist and tongue movement **44**
5.1 Introduction **44**
5.2 Methods **45**
5.2.1 Subjects 45
5.2.2 Tasks 45
5.2.3 Movement onset detection 48
5.2.4 Event related desynchronization (ERD) 50
5.3 Results **51**
5.4 Discussion and Conclusion **52**

Chapter 6 Conclusion and Future Work **54**
6.1 Conclusion **54**
6.2 Future Work **55**
6.2.1 Analysis of brain excitability at the onset of limb and tongue movement 55
6.2.2 TDS-KINARM experiment with EEG and EMG recording 56
6.2.3 Improved Design and Evaluation of Tongue Drive System optimized for capturing precise tongue movement 57

APPENDIX A. List of Publications **63**
A.1 Journal Papers **63**
A.2 Conference Papers **63**

APPENDIX B. Tongue Drive System Development **64**
B.1 Bluetooth based TDS design for KINARM interface **64**
B.2 Initial development of embedded algorithm for Tongue Drive System **69**
B.3 Design of Assistive Manipulation Framework Using Augmented Reality and Tongue Drive System **70**

REFERENCES **72**

LIST OF TABLES

Table 2.1	RMSE Results of Participants in Different Modes	14
Table 3.1	The TDS-KINARM system control modes	23
Table 3.2	Stroke subject demographics and Fugl-Meyer Assessment (FMA) for Upper Extremity	29
Table 6.1	Approximate location and orientation of all magnet sensors. All sensor rotation procedure is using right hand rule. After applying rotation z, y, and x (order matters), the sensor will be in the same coordinate as the global coordinate as shown in Figure 6.4. The rotation angle is positive if the rotation is in the counter-clockwise direction when viewed by an observer looking along the y-axis towards the origin.	58

LIST OF FIGURES

Figure 2.1	TDS-HM system block diagram for external Tongue Drive System (eTDS) paired with the robotic Hand Mentor Pro^{TM} (HM) for upper extremity movement rehabilitation. The words in parenthesis describe how different signals propagate. The dashed arrows indicate visual feedback.	9
Figure 2.2	(a) HM Wrist Exoskeleton. (b) Block diagram of TDS-HM interface connecting the Hand Mentor (HM) rehabilitation robot to a PC and eTDS headset via USB and BLE, respectively.	9
Figure 2.3	Figure 2.3 TDS-HM experiment setup with example sinusoidal target tracking GUI. The green line in the GUI is the user input angle or pressure, and the user is asking to track the green line within the light blue color region.	8
Figure 2.4	(a) An example performance of the pressure sensor readout (solid black line) and the target (dashed blue line). (b) P-1 performance. (c) P-2 performance. (d) P-3 performance.	15
Figure 3.1	Conceptual diagram of the tongue-operated exoskeleton for post-stroke upper limb function recovery. Arm function may potentially be regained through movement initiation of the affected arm by volitional tongue motion under control of the Tongue Drive System (TDS) via KINARM^{TM} exoskeleton, while the patient receives audiovisual feedback.	18
Figure 3.2	Functional block diagram of the TDS-KINARM system	19
Figure 3.3	TDS-KINARM Setup	25
Figure 3.4	Unidirectional reaching task performance outcome in active (A), active with viscous force field (AV), passive (P), discrete tongue control (DT), proportional tongue control (PT), discrete tongue hybrid control (DT_H), and proportional tongue hybrid control (PT_H) modes for the target distance-width pair of 24 cm – 3 cm across 10 healthy subjects. (a)-(d) An examples of arm endpoint trajectories of one subject during reaching using control modes A, AV, DT, and PT, respectively. The regions between the red lines indicate the targets. (e) Completion Rate (CR). (f) Throughput (TP). (e) and (f) bar plots show the mean±SD. The asterisks show significant ($p<0.05$) differences between control modes.	27

Figure 3.5	Tracking task performance outcome (RMSE) for active (A), active with viscous force field (AV), proportional tongue control (PT), and proportional tongue hybrid control (PT_H) modes across 10 healthy subjects. (a) and (b) show examples of the tracking end point location of one healthy subject using A and PT_H control modes with moving target speed of $\boldsymbol{\omega = 0.1}$. (c) and (d) show examples of the mapping of the horizontal end-point position versus time using A and PT_H control modes respectively with moving target speed of $\boldsymbol{\omega = 0.1}$. The blue line indicates the virtual reality mapping of the horizontal endpoint position; the red line indicates the location of the moving target. The region between the green lines indicates the active range of motion without robot assistance. (e) shows the RMSE of each mode with two different speeds calculated across all healthy subjects (mean±SD). The asterisks show significant ($p<0.05$) differences between control modes.	28
Figure 3.6	NASA Task Load Index score for unidirectional reaching task in control mode active (A), active with viscous field (AV), discrete tongue (DT), proportional tongue (PT), discrete tongue hybrid (DT_H), and proportional tongue hybrid (PT_H) across all healthy participants (mean±SD).	30
Figure 3.7	Tracking task performance outcome (RMSE) for proportional tongue hybrid control (PT_H) for stroke subjects. (a) and (b) shows examples of end-point displacements of both stroke subjects during target tracking using proportional tongue hybrid (PT_H) control mode with moving target speed of $\omega=0.1$. (c) and (d) show end-point position as a function of time for stroke subjects #1 and #2, respectively, with moving target speed of $\omega=0.1$ during target tracking. (e) and (f) show the RMSE of both stroke participants for each session with target speed of $\omega=0.1$ and 0.15 respectively.	31
Figure 4.1	Graphic User Interface of Unidirectional Reaching Task. Each participant is asked to move the hand position from initial position to target position with various distance (D) and width (W) pair as quickly and accurately as possible.	36
Figure 4.2	Residual Analysis of end point position in x axis for active control mode. The horizontal axis is the cut off frequency of 2^{nd} order low pass filter apply forward and backward. The vertical axis is the residual in meter.	40
Figure 4.3	Hand kinematics during reaching movements generated by four control modes of the TDS-KA system (A: active control mode, AV: active with viscous field control mode, DT: discrete tongue	43

	control mode, PT: proportional tongue control mode, and PT_T: tongue kinematics in proportional tongue control mode). (a) completion rate with distance-target width pair 24cm-3cm, (b) throughput with distance-target width pair 24cm-3cm, (c) Pearson correlation coefficient between index of difficulty and average movement times, (d) reaction time with distance-target width pair 24cm-3cm (e) jerk cost with distance-target width pair 24cm-3cm, and (f) hand velocity profile symmetry with distance-target width pair 24cm-3cm.	
Figure 5.1	*Left,* Wrist in rest and flexed position on an arm rest with EMG electrode placed in wrist extensor muscle. *Middle*, Wrist in extended position. *Right,* Tongue protrusion with EMG electrode placed above and below opposite corner of the mouth.	46
Figure 5.2	Figure 5.2 Location of EEG electrodes.	47
Figure 5.3	Example of wrist *EMG onset detection starting from differential signal (top left) with the following processing steps: 1.* 6th order Butterworth filter with cutoff frequency of 20Hz (use backward and forward filter to avoid phase distortion) 2. Cut of some samples in the beginning to avoid unwanted noise. 3. Perform Teager-Kaiser operation: $y(i)=x(i)\text{^}2-x(i+1)*x(i-1)$. Full wave rectification. 5. Median filter (256 samples for wrist and 512 samples for tongue). Use the first 2 seconds data as baseline and find the first data point that has crossed the 12th standard deviation for 1024 samples for wrist EMG data. (or the 4th standard deviation for 512 samples for tongue EMG data). The tongue EMG onset time is determined by the average of results from two electrodes.	49
Figure 5.4	Example of event related potential change in EEG for tongue protrusion (t), wrist extension (w), and concurrent tongue protrusion and wrist extension (c) in 10-12 Hz compared with the baseline (from -2.5 to -1.5 s) across trials.	51
Figure 5.5	ERD for wrist extension (w), tongue protrusion (t), and concurrent tongue protrusion and wrist extension (c) for pre-movement (-1.5 to 0 s) and post-movement (0 to 2 s)	53
Figure 6.1	System Block Diagram for TDS-KINARM experiment with EEG and EMG recording.	56
Figure 6.2	TDS-KINARM experiment with EEG and EMG recording. (a) shows the participant sitting in KINARM wearing both EEG cap and TDS system. (b) shows the EMG electrode placement for	57

	elbow flexor and extensor. (c) shows the EMG electrode placement for shoulder extensor.	
Figure 6.3	Enhanced Tongue Drive System Prototype.	59
Figure 6.4	Orientation and location of all sensors are relative to the front surface of the alignment mark on the bottom right corner from user' perspective	60
Figure 6.5	3D magnet positioning platform.	61
Figure 0.1	Flow Chart for TDS sensory signal processing algorithm.	65
Figure 0.2	System Block Diagram of TDS with sensory signal processing algorithm in Mbed MCU.	70
Figure 0.3	Setup of TDS with sensory signal processing algorithm in Mbed™ MCU.	71

LIST OF SYMBOLS AND ABBREVIATIONS

eTDS	external Tongue Drive System
HM	Hand Mentor Pro™
GUI	Graphic User Interface
BLE	Bluetooth Low Energy
PT	proportional tongue control mode
DT	discrete tongue control mode
ERD	Event-Related Desychronization
EEG	electroencephalographic
EMG	electromyographic
BMI	brain-machine interface
FMA	Fugl-Meyer Assessment

SUMMARY

Stroke is a devastating condition that may cause upper limb paralysis. Robotic rehabilitation with self-initiated and assisted movements is a promising technology that could help restore upper limb function. The objective of this research is to develop and evaluate a tongue-operated exoskeleton that will harness the intention of stroke survivors with upper limb paralysis via tongue motion to control robotic exoskeleton during rehabilitation to achieve functional restoration and improve quality of life. Specifically, a tongue operated assistive technology called the Tongue Drive System is used to harness the tongue gesture to generate commands. And, the generated command is used to control rehabilitation robot such as wrist-based exoskeleton Hand Mentor Pro^{TM} (HM) and upper limb-based exoskeleton KINARM^{TM}. Through a pilot experiment with 3 healthy participants, we have demonstrated the functionality of an enhanced TDS-HM with pressure-sensing capability. The system can add a programmable load force to increase the exercise intensity in isotonic mode. Through experiments with healthy and stroke subjects, we have demonstrated that the TDS-KINARM system could accurately translate tongue commands to exoskeleton arm movements, quantify function of the upper limb and perform rehabilitation training. Specifically, all healthy subjects and stroke survivors successfully performed target reaching and tracking tasks in all control modes. One of the stroke patients showed clinically significant improvement. We also analyzed the arm reaching kinematics of healthy subjects in 4 modes (active, active viscous, discrete tongue, and proportional tongue) of TDS-KINARM operation. The results indicated that the proportional tongue mode was a better candidate than the discrete tongue mode for the

tongue assisted rehabilitation. This study also provided initial insights into possible kinematic similarities between tongue-operated and voluntary arm movements. Furthermore, the results showed that the viscous resistance to arm motion did not affect kinematics of arm reaching movements significantly. Finally, through a 6 healthy subject experiment, we observed a tendency of a facilitatory effect of adding tongue movement to limb movement on event-related desynchronization in EEG, implying enhanced brain excitability. This effect may contribute to enhanced rehabilitation outcome in stroke survivors using TDS with motor rehabilitation.

CHAPTER 1 INTRODUCTION

1.1 Background and Motivation

Stroke is the leading cause of adult disability in the United States. Every year, around 795,000 people experience a new or recurrent stroke. An estimated 2.7% of the population in the U.S. is affected by stroke [1]. Between 2012 and 2030, total direct medical stroke-related costs are projected to triple, from $71.b billion to $184.1 billion [1]. Of all the stroke survivors, around three quarters experience different degrees of upper limb paresis, which reduce their quality of life severely [2].

Rehabilitation can help stroke survivors reduce disability and regain their independence [3]. Extensive research has been done to identify the most effective strategies for stroke rehabilitation ranging from movement therapy to complementary medicine [4]. Among promising rehabilitation strategies, robot-assisted rehabilitation has been developed to assist stroke rehabilitation [5]. Compared with traditional therapy, robotic based rehabilitation enables the clinician to deliver more consistent therapy with measurable result in real time [6].

Literature suggests that robotic rehabilitation either has the same or better rehabilitation outcomes compared to traditional therapy [3]. A systematic robotic aided therapy review based on 8 clinical trials from 1975 to 2005 concludes that robot-aided therapy of the upper extremity improves motor control of shoulder and elbow in subacute and chronic patients [7]. However, no consistent influence on functional abilities was found. Further, the rehabilitation outcomes of robot-aided therapy appear to be greater than

conventional therapy. A Cochrane review that includes 34 clinical trials (1160 participants in total) concludes that electromechanical and robot-assisted arm and hand training improves activities of daily living, function and muscle strength in people after stroke [8]. However, the authors noted that the results must be interpreted with caution because the quality of evidence from the existing clinical trials conducted with robotic devices is low to very low, and there are variations between the trials in factors such as intervention intensity, duration, etc.

While robotic rehabilitation that involves moving patients' arm passively may provide some clinical benefits [9], the fact that such interventions have no significant effects on motor control outcome suggests that passive movement from robot alone is not enough, and active participation from patients may bring better clinical outcomes [10]. A robotic rehabilitation that requires active stroke survivor participation while adapting to the patients' motor ability and providing constant challenge (performance-based progressive therapy) provides much better clinical outcome compared to passive robotic training [11]. These results are consistent with the current understanding of the neurobiology of recovery after neurological injury [12][13][14] as well as the current trends in robot-assisted upper-limb stroke rehabilitation [15].

Several human-computer interaction methods have been considered to detect and provide user intent to a rehabilitation robot. These methods include triggering robot assistance based on human arm mechanical variables (force or velocity), movement of the other limb, bioelectric signals via electromyographic (EMG) or electroencephalographic (EEG), or gaze tracking. However, these methods have different types of limitations. Intent detection method based on limb force or velocity is the most intuitive way to control

rehabilitation robot. However, approximately 30 percent of stroke patients have severe upper extremity paresis [2]. Thus, they would have difficulties initiating movement by their affected upper limb [10]. In theory, using the intact limb could promote functional recovery of the impaired limb through coupling effects [16]. However, a Cochrane review reported that there was no significant improvement of bilateral arm training using this method compared with usual care following stroke [17]. This result suggests that using another limb to provide user intent to robot might not produce positive clinical outcome. While EMG can capture electrical activity produced by skeletal muscles, the EMG pattern recognition approach might not be practical to decode movement intention of stroke survivors [18]. EEG-based brain-machine interface (BMI) methods have shown promise in restoring upper extremity motor function in stroke survivors [19][20]. However, the EEG-based BMI may be difficult to use in a rehabilitation setup due to a considerable amount of time and effort it takes for setting up and for training to be functional [21]. A recent study [22] has shown that healthy subjects can use a gaze tracking system to capture intention. However, eye-tracking-based solution needs further improvements and clinical evaluation to be a viable solution.

Tongue motion, if properly harnessed, could be used to communicate human intents to a rehabilitation robot or an assistive device [23][24]. It has several advantages compared with the other methods of intention detection described above. The tongue has a strong representation in the human motor cortex, a direct connection to the brain through cranial nerves, and numerous inherent and intuitive capabilities that can be tapped to overcome the above limitations [25][26]. The tongue can also move rapidly and accurately almost in any directions within the oral space with many degrees of freedom. Access to the tongue

is readily available noninvasively, and its muscle fibers are fatigue-resistant, allowing usage of a tongue-operated rehabilitation system over extended periods of time [27]. Although speech and language are often affected by stroke [28], survivors generally maintain their voluntary tongue control, which makes the tongue a potential vehicle for controlling robotic rehabilitation devices with the patient's own intention. Perhaps the most important observation is that the topographical alterations of the sensorimotor cortex can shift the motor representation of the tongue into the cortical region of the hand representation due to their proximity for people with cervical SCI [29] and congenital absence of one hand [30]. Thus, by engaging both tongue and upper limbs in synchrony, their representations in the primary motor cortex may reorganize and the upper extremity function may improve, thanks to the brain neuroplasticity.

The objective of the proposed research is to develop and evaluate a tongue-operated exoskeleton that will harness the intention of stroke survivors with upper limb paralysis via tongue motion to control robotic exoskeleton during rehabilitation to achieve functional restoration and improve quality of life. Specifically, a tongue operated assistive technology is called the Tongue Drive System is used to control rehabilitation robot such as wrist-based exoskeleton Hand Mentor Pro^{TM} and upper limb-based exoskeleton KINARM^{TM}. In addition to standard clinical outcome measures such as Fugl-Meyer Assessment, we have obtained measurable kinematic result from robots as well as electrical activities of brain and relevant muscles from EEG and EMG, respectively.

1.2 Specific Aims

1.2.1 Specific Aim 1: Enhancement and evaluation of a tongue-operated wrist robotic rehabilitation system

A previous study has demonstrated that the Tongue Drive System could be combined with a wrist rehabilitation robot for stroke rehabilitation. We aim to develop and test an enhanced TDS-HM prototype that includes a BLE eTDS headset, HM Pro^{TM}, and a custom designed interface in the form of a USB dongle. The new TDS-HM has pressure-sensing capability that can add rehabilitation tasks based on isometric mode. The system can add a programmable load force to increase the exercise intensity in isotonic mode. A force protection mechanism was also added to reduce the risk of injury. The tongue-operated isotonic proportional control mode SSP algorithm was improved by adding PWM-based output to the HM motor.

1.2.2 Specific Aim 2: Design and evaluation of a tongue-operated upper limb rehabilitation system

We aim to develop and evaluate a tongue-operated exoskeleton system (TDS-KINARM system) for upper limb rehabilitation. We enhanced a tongue-operated assistive technology called the Tongue Drive System (TDS) and interfaced it with the exoskeleton KINARM^{TM}. We also developed unidirectional target reaching and target tracking tasks with different control modes and tested them in a group of 10 healthy participants (7 males and 3 females, age 23-60 years) and two female stroke survivors with upper extremity impairment (age 32 and 58 years, Fugl-Meyer upper extremity baseline score 35 and 13 out of 66).

1.2.3 Specific Aim 3: Analysis of arm reaching movement controlled by a tongue-operated exoskeleton system: Implications for stroke rehabilitation

In order to design appropriate rehabilitation interventions with the TDS-KINARM system, we examined the arm reaching kinematics (throughput, completion rate, conformity to Fitts' Law, jerk cost, reaction time, and velocity profile) of healthy subjects in 4 modes (active, active viscous, discrete tongue, and proportional tongue) of TDS-KINARM.

1.2.4 Specific Aim 4: Analysis of brain excitability at the onset of wrist and tongue movement

Initiation of voluntary movement accompanies a desynchronization of neural oscillations that are observed in EEG over the sensorimotor cortex (event-related desynchronization). We hypothesize that an addition of voluntary tongue movement enhances brain excitability that is associated with the initiation of limb movement. We would like to examine if event-related desynchronization for the upper-limb area is enhanced with concurrent initiation of tongue and wrist movement in healthy adults.

CHAPTER 2 ENHANCEMENT AND EVALUATION OF A TONGUE-OPERATED WRIST ROBOTIC REHABILITATION SYSTEM

2.1 Introduction

Studies of neuroplasticity indicate that areas of the brain not injured by stroke are able to reorganize neural pathways when actively engaged [12][13][14]. In a previous study [23], we have developed a tongue-operated robotic rehabilitation system (TDS-HM) to harness the tongue voluntary motion through a wireless and wearable assistive technology, called the external Tongue Drive System (eTDS), in the form of a headset, which controls an existing rehabilitation robot, called Hand Mentor (HM).

Through a small pilot study involving several healthy participants and three stroke survivors, we received clinically viable feedback for further improvements. Based on this

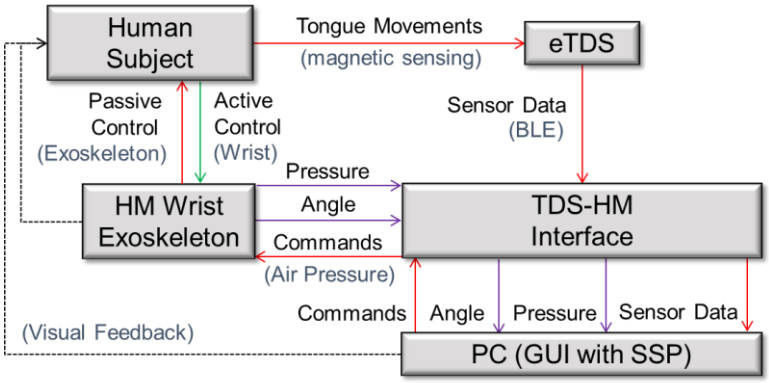

Figure 2.1 TDS-HM system block diagram for external Tongue Drive System (eTDS) paired with the robotic Hand Mentor Pro™ (HM) for upper extremity movement rehabilitation. The words in parenthesis describe how different signals propagate. The dashed arrows indicate visual feedback.

feedback, we have developed an enhanced version of the TDS-HM as shown in Figure 2.1. The new system combines a 2nd generation Hand Mentor Pro™ (HM) with a new version of the eTDS that includes a Bluetooth Low Energy (BLE) transceiver. In addition to the existing capability of reaching the joint angle, the new TDS-HM interface is capable of reading pressure, which is proportional to the force exerted to the user's wrist, from the sensors embedded in the pneumatic actuator of the HM upper limb exoskeleton, as shown in Figure 2.2. A combination of these two sensing modalities allows designing more elaborate tasks and better evaluation of the user performance. In addition to the hardware update, the control of the wrist exoskeleton was enhanced to include pulse width modulation (PWM) of the air pump and releasing valves. Preliminary results in 3 healthy subjects who performed a sinusoidal target tracking task demonstrated the TDS-HM system functionality in hand-operated isometric, hand-operated isotonic, tongue-operated isotonic discrete and tongue-operated isotonic proportional control modes.

2.2 System Description

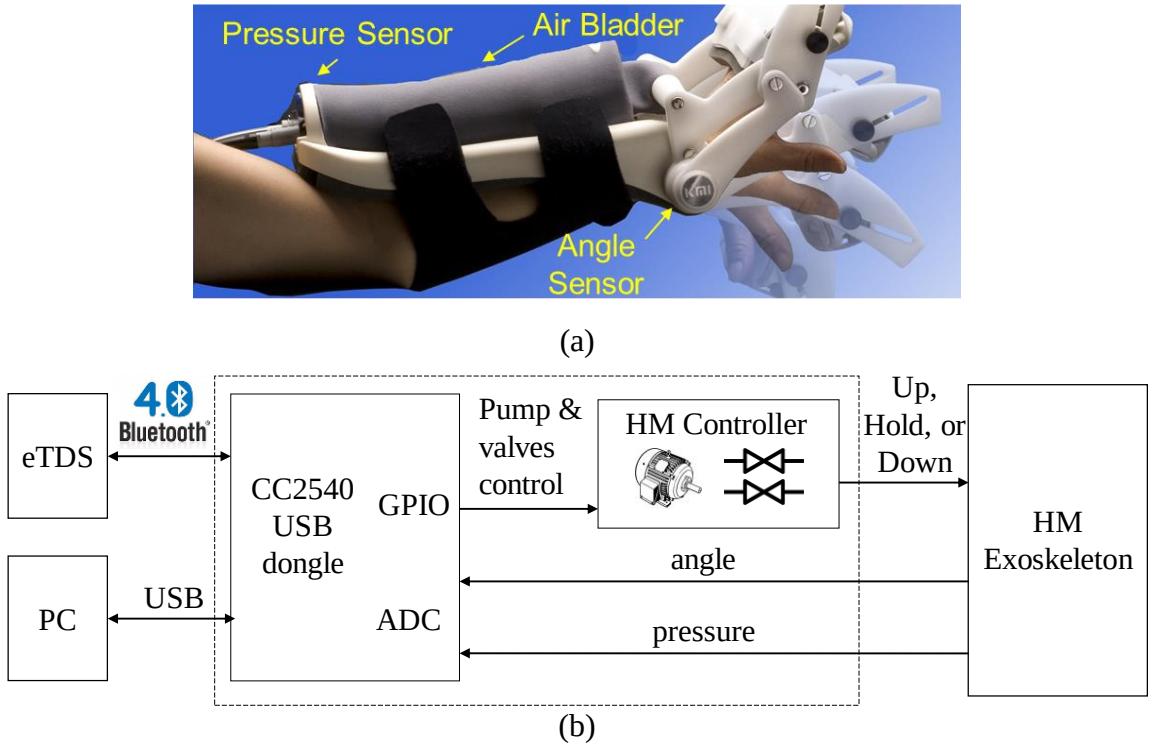

Figure 2.2 (a) HM Wrist Exoskeleton. (b) Block diagram of TDS-HM interface connecting the Hand Mentor (HM) rehabilitation robot to a PC and eTDS headset via USB and BLE, respectively.

2.2.1 BLE Based eTDS Headset

The eTDS is a headset with bilateral extensions that positions an array of four 3-axis magnetic sensors (LSM303D, ST Microelectronics) near the user's cheeks [31]. These sensors are used to locate the position of a magnetic tracer that is temporarily glued to the user's tongue. All the magnetic sensor data, which is sampled at 50 Hz, is delivered to the headset's MCU (CC2541, Texas Instruments) via serial peripheral interface (SPI). The 24-byte packetized sensor data is then sent wirelessly to a PC via the TDS-HM interface for processing by a sensor signal processing (SSP) algorithm that ultimately enables the user to issue a set of predefined tongue commands from different tongue gestures [32]. The usability of the eTDS for computer access and wheelchair navigation had already been

established in clinical trials [33]. Compared with the previous eTDS headsets, which used a proprietary 2.4-GHz radio transceiver, the new BLE eTDS headset provides a more energy efficient, secure, and universal wireless connection between the eTDS and TDS-HM USB dongle.

2.2.2 TDS-HM Interface Design

The TDS-HM Interface and its associated firmware receive both angle and pressure sensor data from HM exoskeleton and magnetometer sensor data from the TDS headset. Figure 2.2 shows the system block diagram of the TDS-HM interface, which consists of a BLE USB dongle (CC2540) and a HM controller. The BLE USB dongle was designed to 1) receive magnetic sensor data from eTDS via BLE wireless link, 2) receive analog angle and pressure signals from HM wrist exoskeleton sensors and digitize them, 3) send the acquired data from TDS and HM as well as the wireless connection status to the PC, 4) receive custom designed connection or reading request from PC, and 5) send PC commands to the HM pump controller. We used a customized communication protocol that included three commands to control the BLE USB Dongle from the LabVIEW based GUI: 1) handshake routine that connects BLE USB Dongle to TDS, 2) data receiving routine that reads magnetic pressure, and angle sensors, and 3) data transmitting routine that sends commands to control HM Wrist Exoskeleton.

The magnetic sensor data from eTDS was received using the notification method as multiple characteristics under one BLE service. Notification was required to be enabled in the handshake stage between the BLE USB dongle and eTDS headset in addition to device discovery, linking device, BLE service/characteristic discovery, and BLE

connection parameter update routines. Since CC2540 had built-in USB communication capability, the UART to USB converter used in the previous TDS-HM Interface was no longer needed.

The HM data acquisition printed circuit board contained the HM controller. We routed the control inputs of the HM to receive commands from BLE USB Dongle. The general purpose input/output (GPIO) pins of the BLE USB dongle were used to drive the MOSFETs that controled the air pump and valves in the HM controller. The wrist angle data was captured by a potentiometer, while the pressure data was acquired by MPX5700 (Freescale). Both angle and pressure sensor data were displayed on the graphical user interface (GUI) that provided the patient with visual feedback.

2.2.3 TDS-HM Control Modes

With the addition of pressure sensor data, TDS-HM could operate in both isotonic and isometric modes. In the isotonic mode, the HM valves were open, and the wrist moves freely while the TDS-HM recorded the corresponding joint angle as the user tracked the target on the GUI. The TDS-HM system could also provide a programmable constant force to the wrist by modulating the valves to increase the intensity of the exercise and wrist workload of the isotonic mode. In the isometric mode, one the other hand, the HM valves were closed and the wrist did not move considerably while the TDS-HM recorded the pressure changes in the actuator bladder, which was proportional to the force applied by the user's wrist, as he/she tracked the target on the GUI. Clinical studies have indicated that both Isometric and Isotonic exercises within active ROM provide valuable rehabilitation outcome [34].

2.2.4 Tasks and Graphic User Interface

A sinusoidal target tracking task was used to evaluate the new TDS-HM. The user needed to move his/her paretic wrist to track the target produced by the GUI. When the user was moving within his/her active range of motion (ROM), the TDS-HM was operated based on the wrist flexion and extension as shown in Figure 2.2(a). When the user needed to move outside his/her active ROM, i.e. within the user's passive ROM, the TDS-HM was operated using the tongue motion, via eTDS commands [23].

TDS-HM GUI was designed to calibrate both eTDS and HM and perform sinusoidal target tracking tasks for all aforementioned modes and controls methods. The minimum and maximum force that the users could apply to the wrist exoskeleton within their active ROM were measured from pressure sensor during calibration. Further, the pressure sensor provided a protection mechanism for the users. In all modes of operation, if the sensed pressure exceeded the maximum pressure recorded in the calibration stage, the system would open the pump outflow valve to reduce the risk of injury.

2.3 Performance Evaluation

A pilot study was conducted with 3 able-bodied volunteers, two male and one female, with ages from 23 to 31 years old. The institutional review board (IRB) approval and informed consent form were received. Figure 2.3 shows the experimental setup. Participants wore the eTDS headset, and a permanent-type magnetic tracer (⌀3 mm × 1.1 mm) was attached to their tongues using tissue adhesive, followed by the eTDS calibration and training procedure, similar to [31]. First, the hand-operated isometric and isotonic modes tracking tasks were performed. For hand-operated isometric task, the pressure level

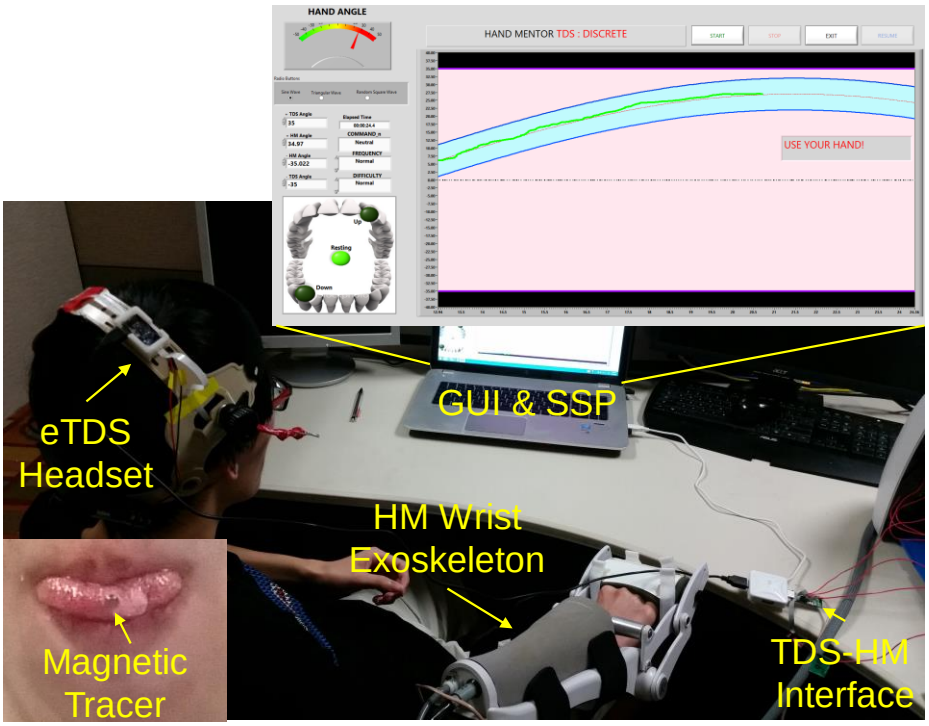

Figure 2.3 TDS-HM experiment setup with example sinusoidal target tracking GUI. The green line in the GUI is the user input angle or pressure, and the user is asking to track the green line within the light blue color region.

was calibrated based on the strength of each participant. For hand-operated isotonic task, the joint angle was calibrated based on the active ROM of each participant. Then, the tongue-operated isotonic discrete control and the tongue-operated isotonic proportional control tasks were performed. For each tongue-operated task, the participants were required to only use their tongue motion to control the HM. Each participant completed one trial for all tasks. Each task took ~5 minutes to complete, and the entire session took 60 to 70 minutes for each participant including magnetic tracer attachment, eTDS/HM calibrations, and four sinusoidal target tracking tasks.

All participants successfully completed the assigned tasks and their performances were measured using root mean square error (RMSE) in target tracking,

$$RMSE_j = \sqrt{\frac{\sum_{i=1}^{n}\left(\frac{I_{ij} - T_{ij}}{\max(T_j) - \min(T_j)}\right)^2}{n}} \quad (1)$$

where n is the number of samples per section, I_{ij} is the input joint angle or pressure data, T_{ij} is the target joint angle or pressure data, i is the index of the input and target data for a particular section, and j is the index of each section.

P-1 had used the TDS-HM system a few times before. P-2 had used the eTDS once, but not the TDS-HM combination. P-3 had neither used the eTDS nor HM before. For each trial, the first 10 s of data were eliminated to account for initial error introduced by the system startup. The remaining data was divided into five sections of 2000 samples each, equivalent to ~40 s. The performance in each task for all participants was evaluated by the mean and standard deviation of the $RMSE_j$ values over all the sections. Table 2.1 summarizes the RMSE results. Figure 2.4a is a tracking example of hand-operated isometric task for P-1 and deviation from the sinusoidal target. Figure 2.4b-d show the RMSE results for each participant. In addition, we were able to program a loaded force in isotonic mode task.

Table 2.1 RMSE Results of Participants in Different Modes

Participant ID	Participant Prior Experience with TDS-HM	RMSE			
		Isometric Mode	Isotonic Mode		
		Hand-Operated	Hand-Operated	Tongue-Operated	
				Discrete Control	Proportional Control
1	Expert	0.022 ± 0.003	0.036 ± 0.010	0.100 ± 0.023	0.094 ± 0.019
2	Novice	0.104 ± 0.034	0.063 ± 0.011	0.227 ± 0.170	0.217 ± 0.183
3	Novice	0.048 ± 0.032	0.031 ± 0.010	0.224 ± 0.068	0.132 ± 0.023

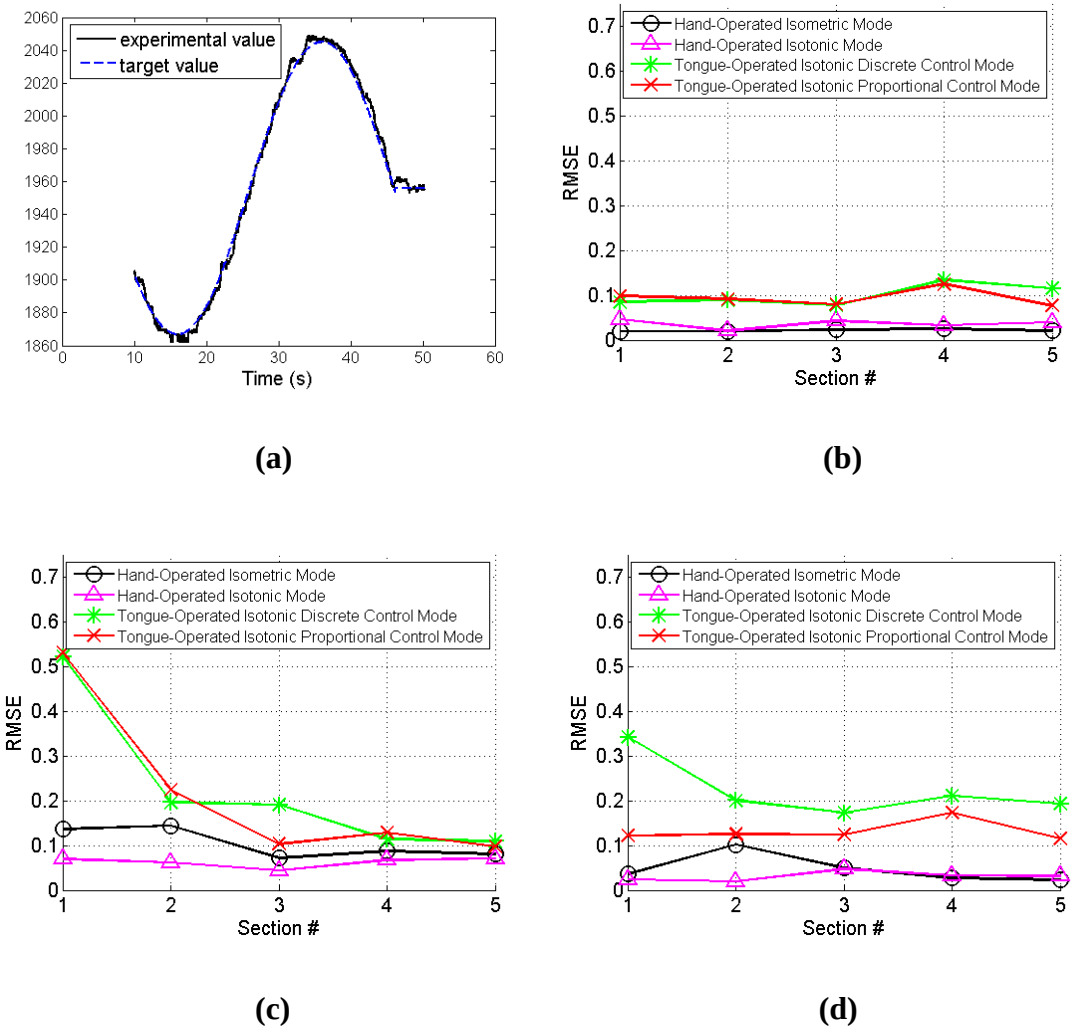

Figure 2.4 (a) An example performance of the pressure sensor readout (solid black line) and the target (dashed blue line). (b) P-1 performance. (c) P-2 performance. (d) P-3 performance.

2.4 Conclusion

We have developed and tested an enhanced TDS-HM prototype that includes a BLE eTDS headset, HM Pro^{TM}, and a custom designed interface in the form of a USB dongle. The new TDS-HM has pressure-sensing capability that can add rehabilitation tasks based on isometric mode. The system can add a programmable load force to increase the exercise intensity in isotonic mode. A force protection mechanism was also added to reduce the risk

of injury. The tongue-operated isotonic proportional control mode SSP algorithm was improved by adding PWM-based output to the HM motor. While this pilot study shows performance improvement for tongue-operated isotonic proportional control mode compared to [23], clinical data from patients with severe hemiparesis is required to determine the real rehabilitative effects of this control mechanism. We also observed that the hand-operated isometric and isotonic modes had comparable performance, and the improved tongue-operated isotonic proportional control mode outperformed the tongue-operated isotonic discrete control mode, in healthy participants.

CHAPTER 3 DESIGN AND EVALUATION OF A TONGUE-OPERATED UPPER LIMB REHABILITATION SYSTEM

3.1 Introduction

In the previous studies, a tongue-operated rehabilitation robot was developed to translate tongue motion to commands via the Tongue Drive system (TDS) [31][35][33][36]. Commands were used to control a wrist-based rehabilitation robot called the Hand Mentor™ [23][37]. This device was shown to elicit improvements in moderate to severely impaired stroke survivors[38][39].

However, the aforementioned study has several shortcomings that could potentially limit clinical outcomes. The Hand Mentor contains only one pneumatic pump that operates one DoF. In addition, it is controlled by an on/off discrete signal. As a result, the robot produces assistive force in only one direction (wrist extension). Due to the on/off switch control, natural and proportionally graded hand movements are not possible.

Thus, it is important to find a more capable rehabilitation robot that can guide stroke patients to move like a healthy person. Furthermore, the potential rehabilitation robot should let stroke patients utilize the Tongue Drive System fully to control their paralyzed upper limb for better rehabilitation outcome. Studies in [40] and [41] provide thorough review on upper limb rehabilitation robots. Of all the options, KINARM is identified as a potential rehabilitation robot to pair with the Tongue Drive System. KINARM™ (BKIN Technologies, Canada) is an exoskeleton that can record kinematics and apply external torques to shoulder and elbow joints in the horizontal plane while providing support against

gravity for both arms [42]. This device has been used in neuroscience research to quantify motor deficits and rehabilitation strategies [43].

The goal of this work is to develop and evaluate a novel tongue-operated upper extremity robotic rehabilitation system (TDS-KINARM) that integrates the TDS and a commercially available bimanual upper extremity exoskeleton KINARM^{TM} (BIKIN Technologies, Canada) as shown in Figure 3.1. An advantage of the KINARM over the Hand Mentor^{TM} is that the KINARM can support weight of the arm and provides movements with two DoF (shoulder and elbow flexion and extension) in a horizontal plane. Here, we present the design of the TDS-KINARM system and preliminary results of its use. We demonstrate the functionality and feasibility of the system using two custom developed tasks with different control modes. We tested these tasks in 10 healthy

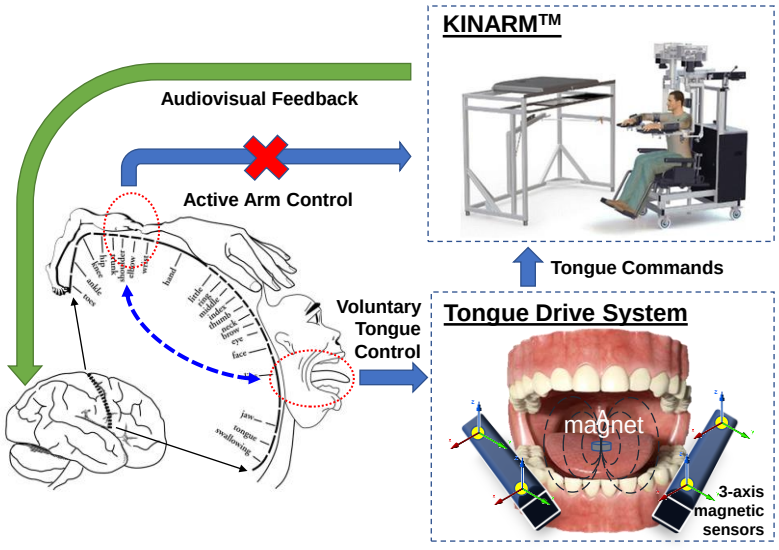

Figure 3.1 Conceptual diagram of the tongue-operated exoskeleton for post-stroke upper limb function recovery. Arm function may potentially be regained through movement initiation of the affected arm by volitional tongue motion under control of the Tongue Drive System (TDS) via KINARM^{TM} exoskeleton, while the patient receives audiovisual feedback.

participants. In addition, we tested a suitable rehabilitation protocol with two stroke survivors.

3.2 Methods

3.2.1 System Description

Our novel paradigm is to actively engage participants by using their own intention via tongue motion to move their upper limb. This device allows us to exam the feasibility of tongue-operated upper limb stroke rehabilitation. In our setup, TDS is used to convert tongue motion to either discrete (rest, left, right, up, or down) [36] or proportional commands (a continuous number from -1 to 1) [44] . These commands are fed into KINARM to control the exoskeleton to complete rehabilitation tasks accordingly.

The TDS consists of a disk-shaped magnetic tracer (D21B-N52, K&J Magnetics, Inc.), a headset with magnetic sensors and transmitter, and a Windows-based PC with an attached USB receiver dongle, as shown on the left side of Figure 3.2. To use TDS, the tracer needs to be attached ~1 cm posterior to the tip of user's tongue via tissue adhesive (Vetbond

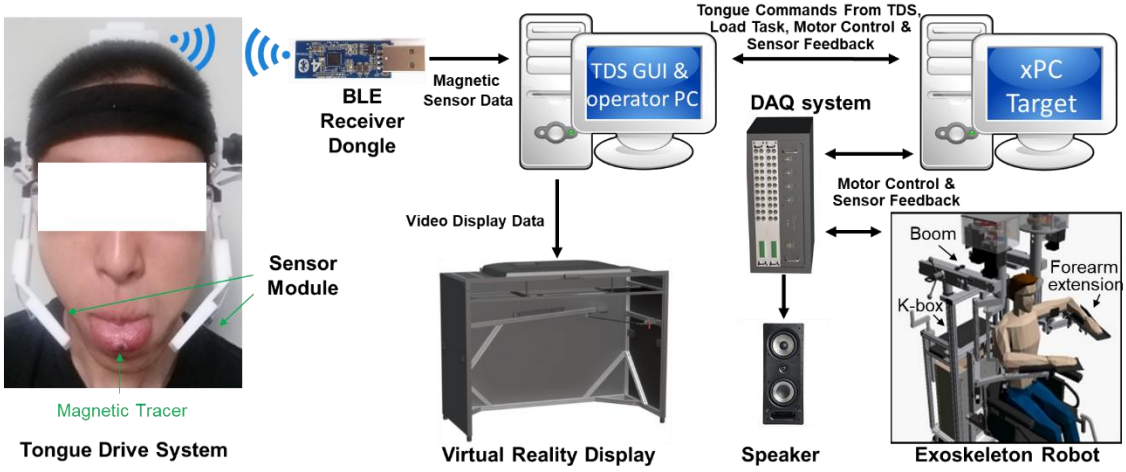

Figure 3.2 Functional block diagram of the TDS-KINARM system

1469Sb, 3M). A LabVIEW (National Instruments) based GUI was developed to control the TDS. Prior to TDS use, external magnetic field (EMF) attenuation procedure should be performed. Subsequently, a pattern recognition algorithm is trained to map tongue gestures and their corresponding magnet flux density fields captured by sensors to discrete or continuous commands. The tongue commands are sampled by KINARM in 200Hz.

Compared to the published description of the system [36], we have made a number of enhancements that makes TDS more robust. We have developed a preprocessing algorithm to eliminate the effects of EMF. Specifically, we have added an additional magnetic sensor in TDS (top sensor) that is away from the magnetic tracer. During the EMF algorithm calibration, we collect data when magnetic tracer is relatively further away from all sensors. In this scenario, all sensors are measuring EMF effectively. Using this data, we can find a transformation matrix that maps the sensor reading of the top magnetic sensor to other magnetic sensors. During normal TDS operation, magnetic sensor reading is subtracted by the transformed top magnetic sensor reading to eliminate unwanted EMF. The TDS training procedure was improved by recording tongue movements while subject is speaking for 10 s. This procedure makes the TDS discrete command robust against activating commands accidentally while speaking. Additional post processing algorithm was added to TDS command output. For discrete commands, the TDS result will only update if the past 10 prediction results are the same. For continuous commands, the TDS result is the average of the past 10 prediction results. This modification makes the TDS output more stable for further robotic control.

KINARM^{TM} (BKIN Technologies Ltd., Canada) is an exoskeleton that can record kinematics and apply external torques to shoulder and elbow joints in the horizontal plane

while providing support against gravity for both arms[42]. This device has been used in neuroscience research to quantify motor deficits and rehabilitation strategies[43]. In our setup, KINARM receive TDS commands via serial to parallel port with a sampling rate of 200Hz. In addition to the standard setup, a speaker is also connected to the analog output port of the data acquisition system to provide audio feedback for the task.

3.2.2 Tasks

Two widely accepted tasks in the human-computer interaction (HCI) and rehabilitation research were adopted and implemented for the TDS-KINARM system. These tasks are unidirectional reaching task (UR) and tracking task (T).

The unidirectional reaching task is based on Fitts' Law [45]. During each trial, the robot brings the participant's hand to initial position. Then, the participant needs to reach any part of a new target (a line of a given width at a given distance) as quickly and accurately as possible using a specific mode. The participant's hand needs to remain on the new target for 1s to register the attempt.

The performance of unidirectional reaching task can be quantified using completion rate (CR) and throughput (TP). CR is defined as the percentage of trials that the participant completed within a certain period (10 s in our case). TP is calculated as [46],

$$TP = \frac{ID}{MT} = \frac{\log_2\left(\frac{D}{W} + 1\right)}{MT} \tag{2}$$

where ID is the index of difficulty, MT is the average time to complete movement, D is the distance to the target, and W is the target width.

The tracking task is based on the previous studies in stroke rehabilitation to evaluate the accuracy of following a moving target [38]. The robot first brings the participant's hand to an initial stationary target. Then, the target starts to move in the left-right direction with a beep. The participant is asked to trace the target as accurately as possible. The position profile of the target is determined by,

$$x_i = x + r \cdot sin(\omega \cdot t) \tag{3}$$

where x is the stationary target position in cm, x_i is the position of the moving target, r = 12 cm is the target displacement radius, ω is an adjustable parameter that determine the speed of movement, t is time in milliseconds.

The performance of the tracking task can be quantified using the root mean square error (RMSE),

$$RMSE = \sqrt{\frac{1}{n}\sum_{i=1}^{n}(x_i - \hat{x}_i)^2} \tag{4}$$

where n is the number of samples, and $\hat{x}_i$ is the horizontal position of the hand.

3.2.3 Control Modes

As shown in Table 3.1, 7 different control modes were developed to move the upper limbs. In the active mode (A, 1), the robot does not provide any resistance or assistance, and the user needs to perform movements using his/her arm. In the active with viscous field mode (AV, 2), the robot provides resistive force as a function of the speed of the upper limb endpoint with an adjustable gain. In the passive mode (P, 3), the robot controls all the movements with an adjustable average movement velocity. In the present experiments, the velocity magnitude was set to v=0.1 m/s. In discrete tongue mode (DT, 4), the robot moves the upper arm in a direction of the tongue command (left, right, forward, backward, or rest) with an adjustable average movement velocity like in the passive mode. The proportional tongue mode (PT, 5) regulates the amount of force applied to the endpoint of the arm with an adjustable gain factor of the tongue command in either the left-right or anterior-posterior direction.

Table 3.1 The TDS-KINARM system control modes

Control Mode	**Description**
Active (A)	No robot load
Active with viscous field (AV)	Robot provides resistive load
Passive (P)	Robot controls all movements
Discrete tongue control (DT)	Use discrete tongue commands to control robot
Proportional tongue (PT)	Use proportional tongue commands to control robot
Discrete tongue hybrid (DTH)	Use discrete tongue commands to control robot based on hand position
Proportional tongue hybrid (PTH)	Use proportional tongue commands to control robot based on hand position

If participants have a limited range of motion, the rehabilitation robot should ideally assist only when needed to maximize rehabilitation outcome [15]. We have developed hybrid modes for both discrete (DT_H, 6) and proportional (PT_H, 7) controls to activate the motors when participants need assistance from the robot outside their active range of motion. In these modes, the participant is instructed to use both arm and tongue control to reach targets for each task. At the same time, the viscous resistive force can be applied to make the task more challenging. For the all healthy subjects' experiments, hybrid region was set to a fixed 6-cm interval. For the stroke participants, the region was set based on the user's range of motion measured before the experiment.

3.2.4 Experimental Protocol

The goal of this study is to perform preliminary evaluation of the tongue-operated upper limb robotic device to study stroke rehabilitation. We demonstrated the functionality and feasibility of the system using two custom developed tasks with different control modes. Specifically, we tested these tasks in 10 healthy right-handed participants (7 males and 3 females between age 23 to 60 years). This experiment with healthy subjects was meant to help us obtain a baseline performance for each task. The setup of the system is shown in Figure 3.3.

During each session, researchers first helped each participant calibrate the TDS. All participants were instructed to perform some baseline TDS related tasks to ensure that they can operate the device. Then, the KINARM was calibrated based on the physical build of each participant. Finally, the participant was asked to perform the custom-made tasks using different control modes.

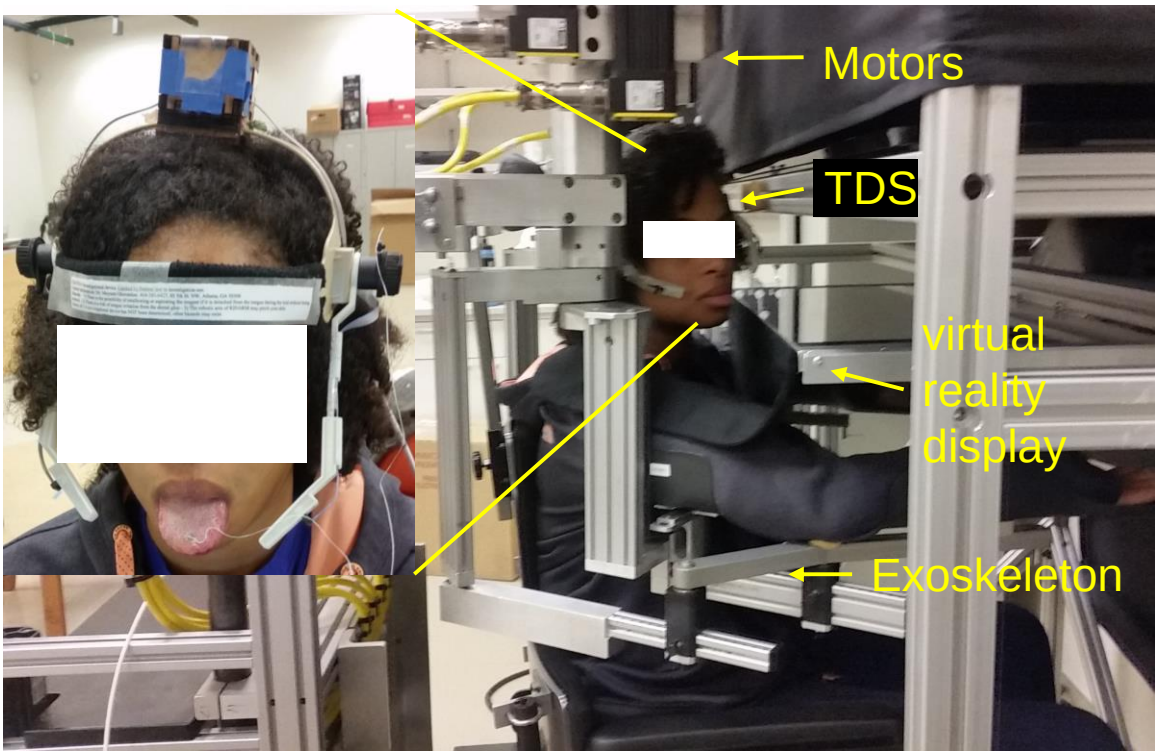

Figure 3.3 TDS-KINARM Setup

We evaluated different control modes through task specific outcome measurement, NASA Task Load Index [47], and user feedback. The NASA task load index (NASA TLX) is a tool for measuring and conducting a subjective mental workload assessment. It rates performance across six dimensions (mental demand, physical demand, temporal demand, effort, performance, and frustration level) to determine an overall workload rating. For this experiment, the score is simplified to a scale of 1 to 5. At the end of each task and control mode combination, we asked questions from NASA TLX, if participant experienced any discomfort, and additional comments.

We characterized each task specific outcome measurement with different control modes by performing Wech's one-way ANOVA and post-hoc Games-Howell test with statistical significance level set to 0.05.

Based on the healthy participants' results, we performed another experiment with two female stroke survivors over six sessions (3 hours each) within two weeks (age 32 and 58 years, Fugl-Meyer upper extremity score 35 and 13). In our experiment, stroke subject #1 had extensive active range of motion for both elbow and shoulder joints. However, stroke subject #2 had almost no active range of motion for elbow joint and limited range of motion for shoulder joint. For the stroke patient experiment, we performed Fugl-Meyer Assessment [48] two weeks before the experiment, right before the experiment, and two weeks after the experiment started.

Both experiments were approved by the institutional Review Board of the Georgia Institute of Technology. Informed consent was obtained to publish the information/image(s) in an online open access publication.

3.3 Results

Each healthy participant performed the unidirectional reaching task with control modes A, AV, P, DT, PT, DT_H, and PT_H (Table 3.1). Reaching distance was 24 cm and target width was 3 cm. Each reaching task was repeated 18 times. Figure 3.4 (panels a-d) displays examples of arm endpoint trajectories of one subject during reaching using control modes A, AV, DT, and PT, respectively. The regions between the red lines indicate the targets. Figure 3.4 (e) and (f) show the completion rate (CR) and throughput (TP). The throughput of DT and DT_H control modes is significantly smaller than the throughput of P, PT, and PT_H control modes ($p = 0.002 – 0.049$). The throughput of P, PT, and PT_H control mode is significantly smaller than throughput of A and AV control modes ($p = 0.002 - 0.006$).

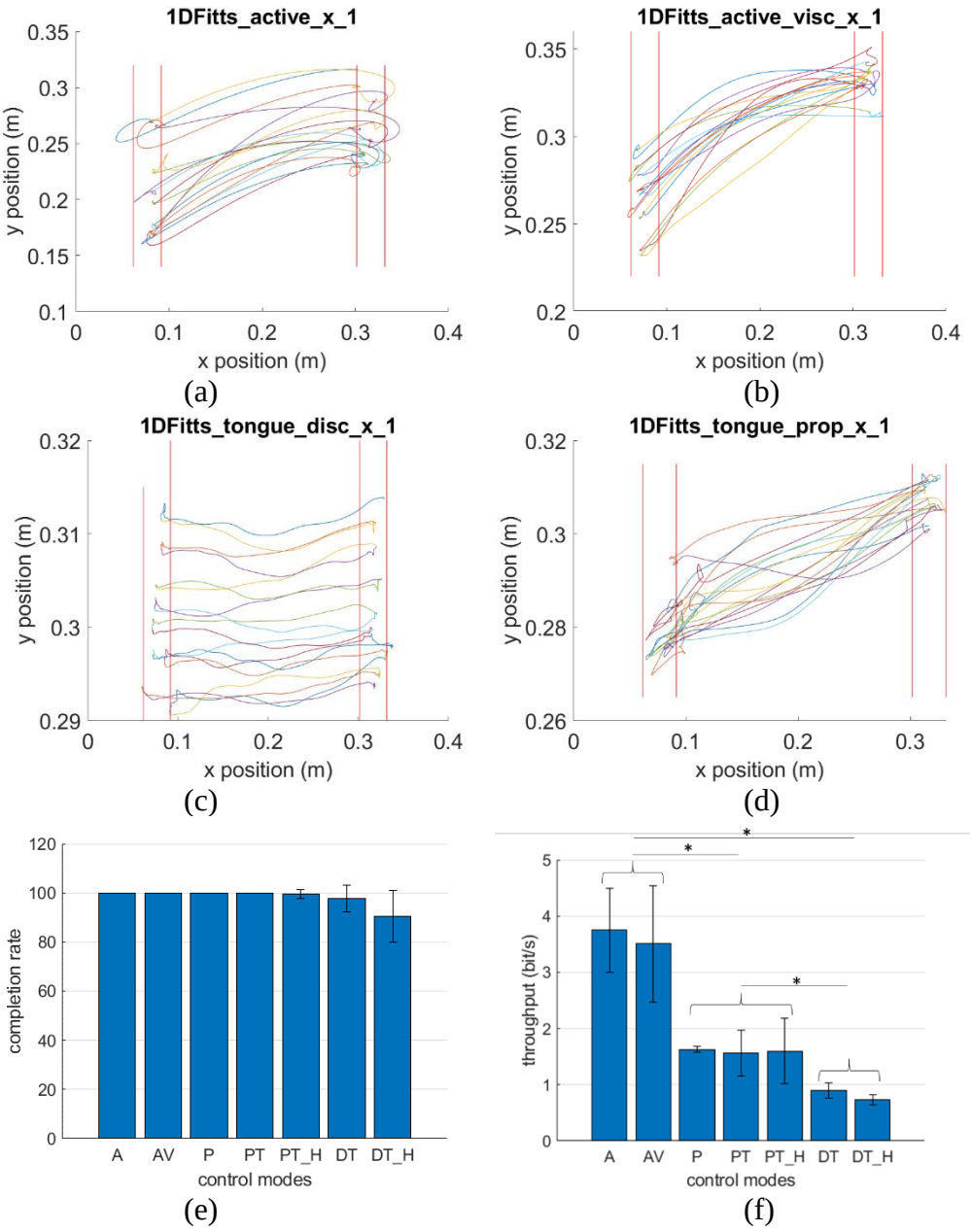

Figure 3.4 Unidirectional reaching task performance outcome in active (A), active with viscous force field (AV), passive (P), discrete tongue control (DT), proportional tongue control (PT), discrete tongue hybrid control (DT_H), and proportional tongue hybrid control (PT_H) modes for the target distance-width pair of 24 cm – 3 cm across 10 healthy subjects. (a)-(d) An examples of arm endpoint trajectories of one subject during reaching using control modes A, AV, DT, and PT, respectively. The regions between the red lines indicate the targets. (e) Completion Rate (CR). (f) Throughput (TP). (e) and (f) bar plots show the mean±SD. The asterisks show significant ($p<0.05$) differences between control modes.

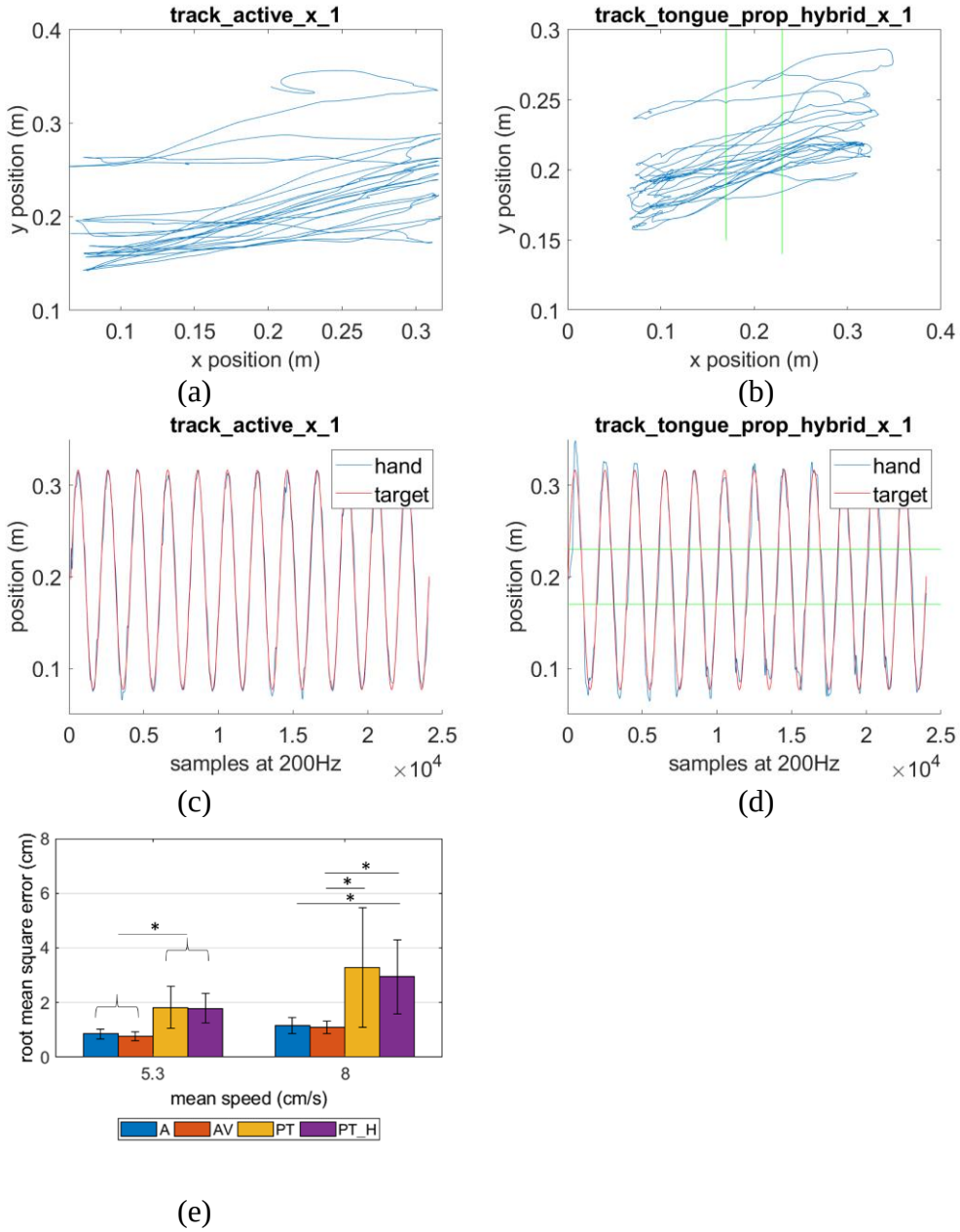

Figure 3.5 Tracking task performance outcome (RMSE) for active (A), active with viscous force field (AV), proportional tongue control (PT), and proportional tongue hybrid control (PT_H) modes across 10 healthy subjects. (a) and (b) show examples of the tracking end point location of one healthy subject using A and PT_H control modes with moving target speed of $\omega = 0.1$. (c) and (d) show examples of the mapping of the horizontal end-point position versus time using A and PT_H control modes respectively with moving target speed of $\omega = 0.1$. The blue line indicates the virtual reality mapping of the horizontal endpoint position; the red line indicates the location of the moving target. The region between the green lines indicates the active range of motion without robot assistance. (e) shows the RMSE of each mode with two different speeds calculated across all healthy subjects (mean±SD). The asterisks show significant ($p<0.05$) differences between control modes.

Each healthy participant also performed the tracking task with two different speeds: $\omega = 0.1$ (mean speed of 5.3 cm/s) and $\omega = 0.15$ (mean speed of 8 cm/s) using control modes A, AV, PT, and PT_H . Figure 3.5 (panels a-b) show examples of the tracking end point location of one healthy subject using A and PT_H control modes with moving target speed of $\omega = 0.1$. Although the tongue control mode PT_H demonstrated some undershoot and overshoot compared to the active arm mode A, the tracking errors were rather small. Figure 3.5 (panels c and d) show the examples of mapping of the horizontal end-point position versus using A and PT_H control modes respectively with moving target speed of $\omega = 0.1$. Figure 3.5 (e) shows the RMSE of each mode with two different speeds calculated across all healthy subjects. It can be seen that the higher speed had higher RMSE values, on average. And PT and PT_H modes have higher RMSE values than A and AV modes (p = 0.003-0.016 for $\omega = 0.1$ and p=0.011 – 0.056 for $\omega = 0.15$).

All participants reported a good acceptance of the system. Figure 3.6 shows the average score of NASA Task Load Index with all control modes. Physical demand and perceived performance of tongue based operating control modes (DT, PT, DT_H, PT_H) are less than for the active control mode (A, AV), on average.

Table 3.2 Stroke subject demographics and Fugl-Meyer Assessment (FMA) for Upper Extremity

Subject	Stroke Type	Gender	Affected Arm	Time since stroke (month)	Age	Baseline FMA	Start Experiment FMA	End Experiment FMA
1	Hermorrhagic	Female	Right	27	32	35/66	38/66	37/66
2	Hermorrhagic	Female	Left	62	58	13/66	12/66	20/66

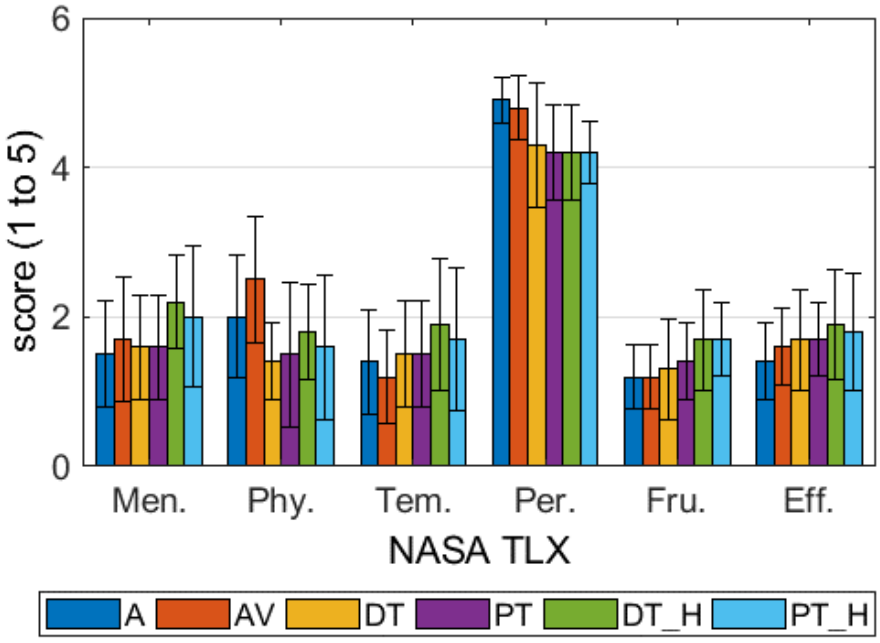

Figure 3.6 NASA Task Load Index score for unidirectional reaching task in control mode active (A), active with viscous field (AV), discrete tongue (DT), proportional tongue (PT), discrete tongue hybrid (DT_H), and proportional tongue hybrid (PT_H) across all healthy participants (mean±SD).

The effectiveness of the tongue-operated upper limb robotic device was evaluated in two chronic stroke patients with moderate (stroke subject #1) and severe (stroke subject #2) paralysis. Both participants reported a good acceptance of the system. Table 3.2 shows relevant patient demographics and clinical outcome. During the control period which was two weeks before the experiment, both participants did not have clinically significant changes in their FMA score [49]. During the experiment period, stroke subject #2 had clinically significant FMA score increase from 12 to 20. Panels a-b in Figure 3.7 shows examples of end-point displacements of both stroke subjects during target tracking with moving target speed of $\omega = 0.1$. Panels c-d in Figure 3.7 show end-point position as a

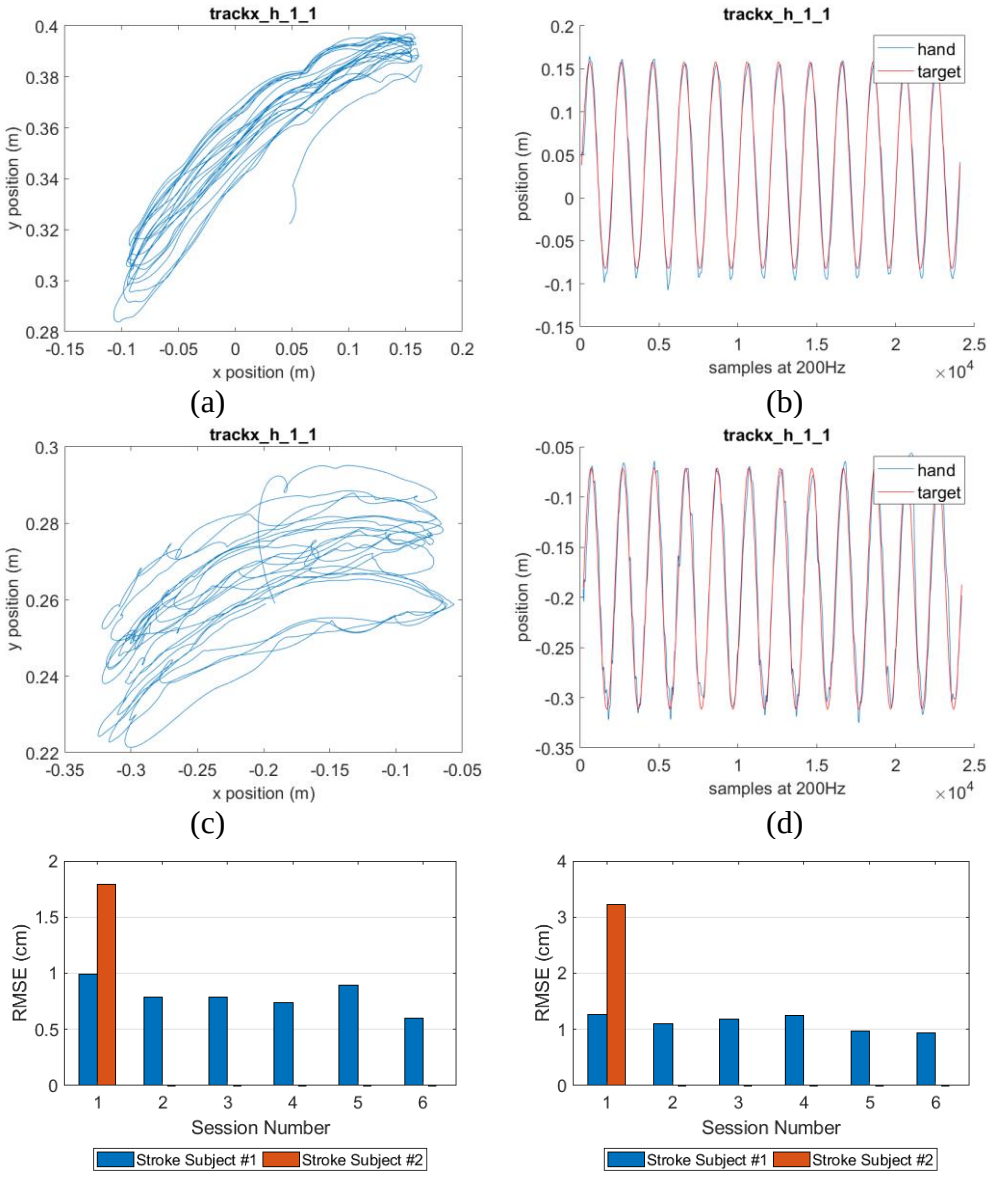

Figure 3.7 Tracking task performance outcome (RMSE) for proportional tongue hybrid control (PT_H) for stroke subjects. (a) and (b) shows examples of end-point displacements of both stroke subjects during target tracking using proportional tongue hybrid (PT_H) control mode with moving target speed of ω=0.1. (c) and (d) show end-point position as a function of time for stroke subjects #1 and #2, respectively, with moving target speed of ω=0.1 during target tracking. (e) and (f) show the RMSE of both stroke participants for each session with target speed of ω=0.1 and 0.15 respectively.

function of time for stroke subjects 1 and 2, respectively, with moving target speed of $\omega = 0.1$. Panels e-f in Figure 3.7 show the RMSE of both stroke participants for each session with target speed of $\omega = 0.1$ and 0.15 respectively. We can also observe that the performance of tracking slower target is better. Also, the performance of stroke subject #1 is higher.

1.1 Discussion and Conclusion

In this study, we presented a novel tongue-operated exoskeleton system to study upper limb rehabilitation. We have evaluated the system with two custom made tasks in 10 healthy participants and 2 stroke participants.

The significant performance difference between the active and tongue-operated control modes indicates that the existing tongue control is still limited. One possibility could be that the participants have not learned fully to use the tongue to control the upper limb. We need to perform a longer-term study in the future. Another possibility could be caused by the maximum force limit set for safety reasons.

We also note that the performance of proportional tongue control mode was significantly better than the performance of discrete tongue control mode. This suggests that the current control outputs offered by the discrete tongue control are limited. For discrete control, the tongue can only issue commands to move the upper limb endpoint with a fixed average velocity. In contrast, the proportional tongue control mode regulates the amount of force applied to the endpoint of the arm proportional to the tongue's relative position.

Although the performance of active and active with viscosity control mode was not significantly different as shown in Figure 3.4 (e), we noted through upper limb end-point position that the applied viscous resistance force has made the movement more precise with less overshoot at the expanse of movement speed as shown in Figure 3.4 (a) and (b).

Based on the questionnaire of subjective perception of the performance (NASA TLX), majority of the subjective performance metrics were comparable, and no statistical significance was found. This result suggests that the active and tongue control modes may be comparable. However, the physical demands and perceived performance of the tongue based operating control modes (DT, PT, DT_H, PT_H) were evaluated to be lower than for the active control modes (A, AV), on average. The physical demand difference is expected because in the tongue control modes, KINARM^{TM} robot is assisting with upper limb movement. Since each participant was more familiar with active control mode, the perceived performance for the active control modes were higher.

We observed that only stroke subject #2 had a clinically significant improvement after the six three-hour experiment sessions. This result suggests that the tongue-operated upper limb rehabilitation paradigm may be beneficial for participants with limited shoulder and elbow active range of motion.

Overall, the developed tongue-operated robotic system has several novel features. First, the system is the first to offer a way to assist in elbow and shoulder joint movements and rehabilitation via the tongue control. Additionally, this study included several practical and reliability improvements for the Tongue Drive System. Prior to this study, the TDS could not reliably provide stable control output especially in proportional control mode.

Although the system has demonstrated some promise for improving therapeutic outcomes in one stroke survivor, more patient data are necessary to fully evaluate the impact of training with this system. Furthermore, monitoring of brain activity can be added to investigate the effects of tongue-controlled upper limb movements on possible neuroplastic changes in the brain. The tongue control currently provided only discrete and 1D proportional control. By expanding the capability of TDS to 2D proportional control, the system can perform more complex tasks.

CHAPTER 4 ANALYSIS OF ARM REACHING MOVEMENT CONTROLLED BY A TONGUE-OPERATED EXOSKELETON SYSTEM: IMPLICATIONS FOR STROKE REHABILITATION

4.1 Introduction

Overcoming kinematic and muscle redundancy of the musculoskeletal system has been considered the central problem of motor control [50]-[54]. In a single upper extremity, there are 30 kinematic degrees of freedom (DOF), including major 7 DOF – 3 in the shoulder (flexion-extension, abduction-adduction, supination-pronation), 2 in the elbow (flexion-extension, supination-pronation) and 2 in the wrist (flexion-extension, supination-pronation), as well as over 66 muscles and muscle compartments that act on these DOF (e.g., [55]). It has been suggested that the central nervous system simplifies motor control by combining individual kinematic DOFs and muscles into groups called kinematic and muscle synergies [50], [51], [56], [57]. Examples of kinematic synergies of arm reaching movements include a straight-line trajectory and bell-shaped velocity profile of the hand [58], a strong association of hand velocity and path curvature [59], and Fitts's law [60] – a strong correlation between the reaching task difficulty and movement time. However, it is unknown if the kinematics movement of the upper limb controlled by the tongue follows similar kinematics synergies.

In Chapter 3, I have described the design and evaluation of a tongue-operated upper limb rehabilitation system. Our working hypothesis is that the voluntary initiation and control of movement in the paretic arm by the normally functioning tongue may help

improve arm motor function. The close proximity of brain representations of the tongue and arm may also contribute to arm functional recovery [29][30]. In order to design appropriate rehabilitation interventions with the TDS-KINARM system, we need to understand more about the kinematic movement of upper limb controlled by the tongue. This chapter closely examines the arm reaching kinematics of healthy subjects in 4 modes (active, active viscous, discrete tongue, and proportional tongue) of TDS-KINARM.

4.2 Methods

All experimental procedures were approved by the Georgia Tech Institutional Review Board. Informed consent was obtained to publish the information/image(s) in an online open access publication. A group of healthy participants (n=10) of both sexes (23-60 years old, 7 males and 3 females) were instructed to perform multiple accurate and fast unidirectional left-right reaching movements between two anterior-posterior lines of different width and distance as shown in Figure 4.1.

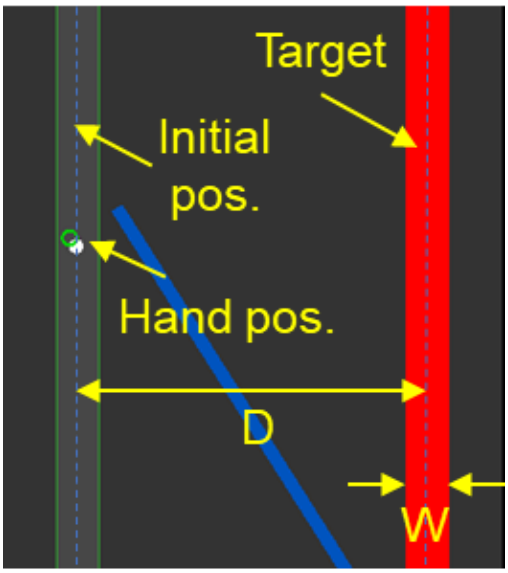

Figure 4.1 Graphic User Interface of Unidirectional Reaching Task. Each participant is asked to move the hand position from initial position to target position with various distance (D) and width (W) pair as quickly and accurately as possible.

Four movement modes were tested: (A) the dominant right arm movement (active control), (AV) active control with viscous resistance, (DT) the relaxed arm moved by the TDS-KINARM system via the tongue motion (discrete tongue control) and (PT) proportional tongue control. Mode A corresponds to a normal arm movement. In mode AV, the robot generates resistive force as a function of the arm endpoint velocity. In mode DT, a discrete command (left or right) is issued by the tongue and the robot moves the arm endpoint in the corresponding direction with an average velocity of 0.1 m/s and bell shaped velocity profile to the end of movement range. When the command is interrupted, the robot will come to a stop as velocity decreases linearly. In mode PT, the instantaneous tongue position is mapped to the force applied to the endpoint of exoskeleton arm. More details can be found in 3.2.3 .

During each session, researchers first helped each participant calibrate the TDS. Then, the KINARM^{TM} was calibrated based on the physical build of each participant. We recorded tongue tip kinematics using a disk-shaped magnetic tracer glued to the tongue tip and magnetic sensors mounted on a headset.

For each subject, a total of 18 trials were collected for each of 4 modes and each reaching distance-target width pair: 24 cm-3 cm, 24 cm-1.5 cm, 12 cm-3 cm, and 12 cm-1.5 cm. Hand kinematics were characterized by completion rate, throughput , reaction time, arm endpoint jerk cost, conformity to Fitts' Law [46] and symmetry of the arm endpoint velocity profile.

Throughput was computed using equation (2) in 3.2.2 . This quantification measurement was developed to measure or quantify human performance of target reaching tasks using an information metaphor.

Fitts' law is a predictive model of human movement primarily used in human–computer interaction and ergonomics. This scientific law predicts that the time required to rapidly move to a target is a function of the ratio between the distance to the target and the width of the target. Index of difficulty shown in equation (2) is function of ratio between the distance to the target and the width of the target. It is used to quantify the difficulty of a specific reaching task. Index of difficulty is higher if the distance to the target is large and the width of the target is small. Conformity of Fitts' Law can be computed using Pearson correlation coefficient between index of difficulty and average movement time. For each participant and mode, the Pearson correlation coefficient is computed as the average of all trials within 1 standard deviation. Then, the Person correlation coefficient for each mode is quantified by computing the mean and standard deviation across all subjects.

Jerk cost has been used to quantify the smoothness of movement [61]. For each trial with different modes and distance width pair, jerk cost is computed using the following formula over the time when the robotic endpoint is moving:

$$\text{Jerk Cost} = \log_{10} \frac{1}{2} \sum j_x^2 + j_y^2 \tag{5}$$

where j_x and j_y are jerks in x and y direction, respectively. For each participant and mode, jerk cost is computed as the average of all trials within 1 standard deviation. Then, the jerk

cost for each mode is quantified by computing the mean and standard deviation across all subjects.

Since the end-point position data fluctuate slightly due to noise, some pre-processing steps are necessary to obtain jerk measurement. I used residual analysis described in [62] to find the optimal cut off frequency. First, the filtered position data were obtained using different cut off frequency from 1 to 20 Hz. I used 2nd order Butterworth filter. The filter was applied both forward and backward to achieve zero phase distortion. Then, the residual value was computed with the equation below:

$$R(f_c) = \sqrt{\frac{1}{N}\sum_{i=1}^{N}\left(X_i - \hat{X}_i\right)^2} \tag{6}$$

where f_c is the cut off frequency for the filter, X_i is the raw position data, $\hat{X}_i$ is the filtered data. After viewing residual for all modes of operation as shown in Figure 4.2, I decided to use 6 Hz as cut off frequency. Once the end-point position data were filtered with optimal cut off frequency, velocity was computed as the derivative of position. Acceleration as computed as the derivative of velocity. And, jerk was computed as the derivative of acceleration.

Previous study has found that unrestrained human arm movement between point targets has an invariant tangential velocity profile when normalized for speed and distance [63]. The velocity profile invariance of speed and load is interpreted as simplification of the underlying arm dynamics [54]. Endpoint velocity symmetry can be used to capture the velocity profile invariance. Specifically, endpoint velocity symmetry was computed as the

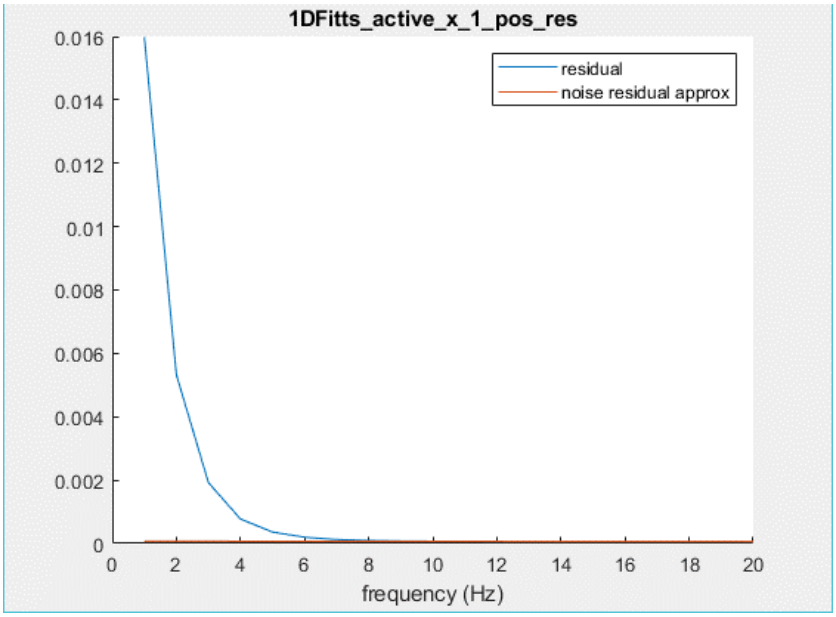

Figure 4.2 Residual Analysis of end point position in x axis for active control mode. The horizontal axis is the cut off frequency of 2nd order low pass filter apply forward and backward. The vertical axis is the residual in meter.

ratio between the time of movement to the peak magnitude of velocity and the time of movement onset (5% of peak magnitude of velocity). The same pre-processing filtering step for end point position data was done to calculating velocity. For each mode and distance width pair, endpoint velocity symmetry was computed as the average of all trials within 1 standard deviation. Then, the endpoint velocity symmetry for each mode was quantified by computing the mean and standard deviation across all subjects.

The endpoint velocity symmetry of the tongue movement was also captured during proportional tongue control mode (PT_T). In proportional mode, the tongue generated command from -1 to 1. The tongue command went through the same processing step as the end point position data.

Previous study [64] has found that simple reaction time averaged 220 ms. In this study, reaction time was measured between time of the audio cue to the time the speed of

movement reaching 5% of peak magnitude of velocity. For each mode and distance width pair, reaction time was computed as the average of all trials within 1 standard deviation. Then, the reaction time for each mode was quantified by computing the mean and standard deviation across all subjects.

We characterized each kinematic outcome measurement with different control modes across all participants by performing Wech's one-way ANOVA and post-hoc Games-Howell test with statistical significance level set to 0.05.

4.3 Results

Nearly all trials were completed within allocated time (10 s) (Figure 4.3 a). The throughput and jerk cost in PT mode were greater than in DT mode and closer to those in A and AV modes although still smaller ($p<0.05$, Figure 4.3 b, e). The lower jerk cost in DT mode compared with other modes could be explained by the fact that the hand velocity profile in DT mode is programmed to have bell shape. And, the speed will change gradually if a command change is detected. This design allows the movement to move smoothly which translates to lower jerk cost.

The Pearson coefficients of correlation between indexes of difficulty and average movement times were between 0.86 and 0.93 for all modes of operation, conforming Fitts' Law (Figure 4.3c). This result confirms that all four control modes conform with the Fitts' Law.

The reaction time for A, AV, and PT modes were similar to the previous study (around 220 ms). However, the reaction time for DT mode is significantly higher (660ms

±137ms, $p<0.05$, Figure 4.3 d). This discrepancy can be partially explained by the fact that it takes around 200 ms to change a command for the Tongue Drive System.

Velocity profile of PT mode was comparable to A and AV modes with symmetry relatively close to 0.5 (equal times of the velocity increase and decrease), whereas DT profile was highly assymetric ($p<0.05$, Figure 4.3f). This discrepancy can also be explained by the design of DT mode. Specifically, the movement speed will change once a command change is detected. In a simple case of reaching to a target on the right, the participant will first issue a right command. At this time, the robot begins to bring the arm to the right edge of the augmented reality screen. Once the target is about to reach, the participant will issue rest command which will cause the robot to reduce speed to rest. As a result, the final speed profile will change from bell shaped velocity profile to a skewed velocity profile towards the end which is reflected in the velocity symmetry skewed towards 1.

4.4 Conclusion

In this study, we have characterized arm reaching kinematics in 4 modes of TDS-KINARM operation. We found that the PT mode is more similar to A and AV modes compared to DT. This result indicates that the PT control strategy is a better candidate than the DT for the tongue assisted rehabilitation. This study also provides initial insights into possible kinematic similarities between tongue-operated and voluntary arm movements. Furthermore, the results show that the viscous resistance to arm motion does not affect kinematics of arm reaching movements significantly.

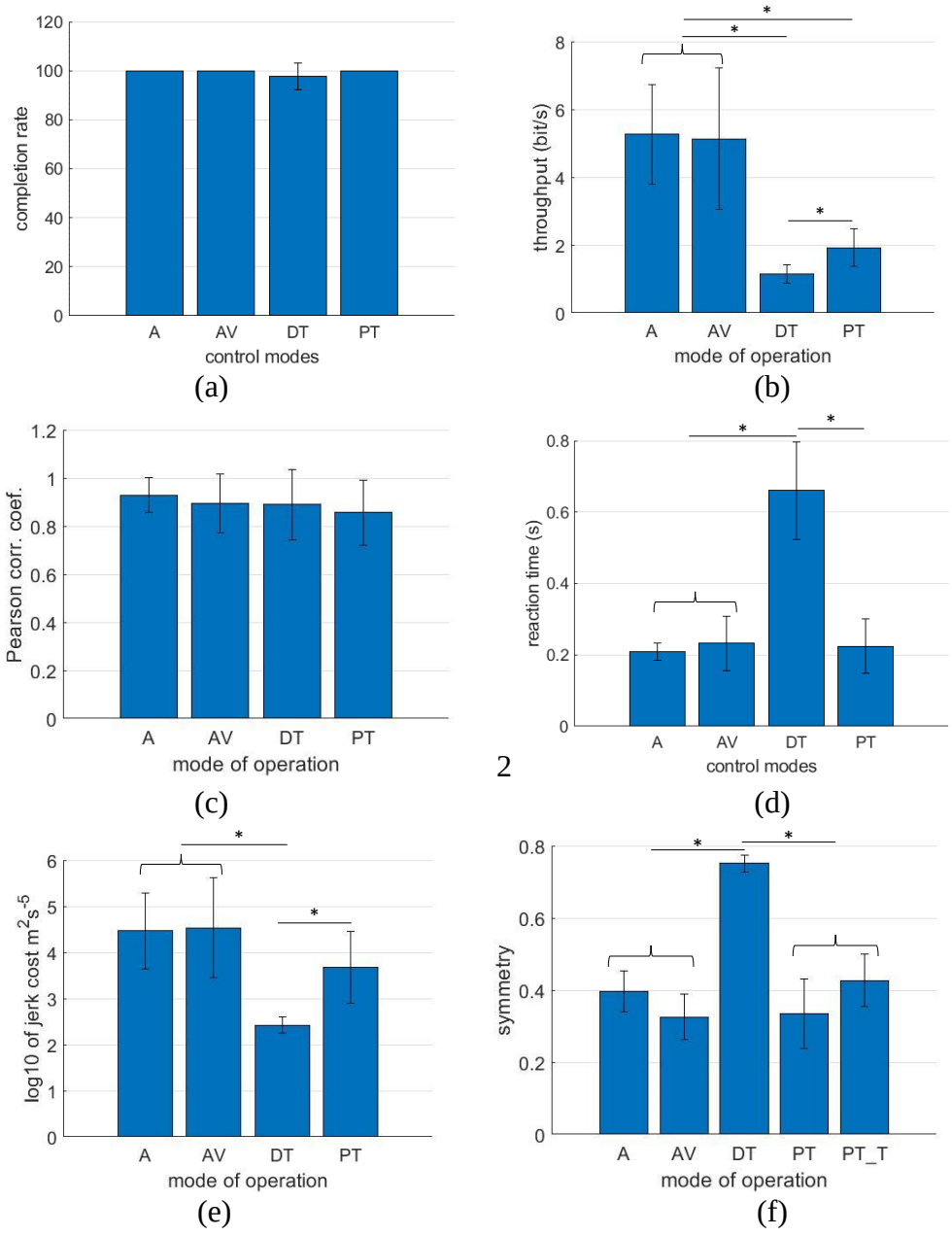

Figure 4.3 Hand kinematics during reaching movements generated by four control modes of the TDS-KA system (A: active control mode, AV: active with viscous field control mode, DT: discrete tongue control mode, PT: proportional tongue control mode, and PT_T: tongue kinematics in proportional tongue control mode). (a) completion rate with distance-target width pair 24cm-3cm, (b) throughput with distance-target width pair 24cm-3cm, (c) Pearson correlation coefficient between index of difficulty and average movement times, (d) reaction time with distance-target width pair 24cm-3cm (e) jerk cost with distance-target width pair 24cm-3cm, and (f) hand velocity profile symmetry with distance-target width pair 24cm-3cm. The asterisks show significant ($p<0.05$) differences between control modes.

CHAPTER 5 ANALYSIS OF BRAIN EXCITABILITY AT THE ONSET OF WRIST AND TONGUE MOVEMENT

5.1 Introduction

Electroencephalography (EEG) is an electrophysiological monitoring method to record electrical activity of the brain. It has been used for functional assessment of chronic hemiparetic patients [65]. Specifically, the amplitude of motor potential, event-related desynchronization (ERD) level has been associated with function improvement measurements such as efficiency, number of peaks in velocity profile, and force mean. To quantify ERD, a number of event-triggered EEG trials are necessary, including some seconds before and some seconds after the event. Electromyography (EMG) is an electrodiagnostic medicine technique for evaluating and recording the electrical activity produced by skeletal muscles. It has been used to monitor muscle synergy changes as an alternative way to measure impairment level [66]. It can be used as an event trigger to study ERD [67].

Voluntary movement results in a circumscribed desynchronization in the upper alpha and lower beta bands, localized over sensorimotor areas. This desynchronization may reflect a mechanism responsible for selective attention focused to a motor subsystem. This effect of focal attention may be accentuated when other cortical areas, not directly involved in the specific motor task, are "inhibited." In this process, the interplay between thalamocortical modules and the corresponding reticular nucleus neurons that forms a

chain of inhibitory neurons that project not only to the thalamocortical relay neurons, but also to neighboring inhibitory neurons may play an important role [68].

As described in the Chapter 3, a tongue-operated rehabilitation robotic system was developed, in which limb movement is assisted by an exoskeleton that is commanded by voluntary tongue motion (Tongue Drive System, TDS). The engagement with this system involves intention of initiating a concurrent motion with the tongue and limb. We hypothesized that an addition of voluntary tongue movement enhances brain excitability that is associated with the initiation of limb movement. The purpose of this chapter was to examine if event-related desynchronization for the upper-limb area is enhanced with concurrent initiation of tongue and wrist movement in healthy adults.

5.2 Methods

5.2.1 Subjects

All experimental procedures were approved by the Georgia Tech Institutional Review Board. Informed consent was obtained to publish the information/image(s) in an online open access publication. Six healthy participants (20-26 years old, 2 males and 4 females) participated in this study.

5.2.2 Tasks

Each participant performed three different motor tasks: tongue protrusion, wrist extension with the right arm, and concurrent initiation of the tongue protrusion and wrist extension as shown in Figure 5.1. Each task had 50 trials, and the tasks were performed in pseudo random order across subjects.

Figure 5.1 *Left,* Wrist in rest and flexed position on an arm rest with EMG electrode placed in wrist extensor muscle. *Middle,* Wrist in extended position. *Right,* Tongue protrusion with EMG electrode placed above and below opposite corner of the mouth.

The onset of wrist and tongue movements was detected from EMG recorded from the wrist extensor muscle and the above and below opposite corners of the mouth, respectively. The brain activity was monitored with 16 electrodes as shown in Figure 5.2. Please note that majority of the electrodes were placed in the motor cortex area except the electrode in FP2 position. FP2 electrode was used to capture eye blinking artifact. Both EMG and EEG signals were captured using ActiveTwo^{TM} in 2048 Hz (BioSemi Instrumentation, Netherland).

During each session, researchers first obtained consent from each participant. Then, researchers placed appropriate EEG cap on based on the participant's head circumference. Then, the cap was adjusted to the proper position. Specifically, researcher measured the nasion-inion and LPA-to-RPA distance and adjusted the vertex (Cz) to be the intercept between two measurements. Then, all electrodes were attached to the corresponding

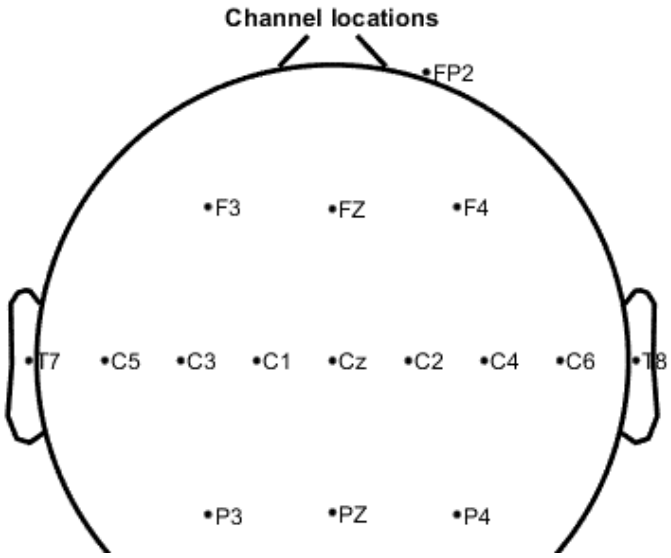

Figure 5.2 Location of EEG electrodes.

location described above after applying gel for electrical contact. Before the experiment started, researcher ensured that all electrodes had stable offsets across channels (< 40 mV).

Once the system setup was complete, each participant was asked to perform the motor tasks in pseudo random order. That is, each participant performed 3 sets of tasks in different orders. At the beginning of each trial, the participant had their right forearm rested with the flexed wrist on an arm rest as shown in Figure 5.1. During each trial, the researchers started recording when the participant indicated he or she was ready with a thumb up gesture. The participant was instructed to perform the motion voluntarily after at least 4 seconds and up to 10 seconds. Once the motor task was completed, both EEG and EMG would be recorded for at least 4 more seconds. Then, the researchers would stop recording and asked the participant to relax and prepare for the next recording.

5.2.3 Movement onset detection

The movement onset was first extracted using a series of steps as shown in Figure 5.3. Once the raw EMG data was extracted and converted to unit in uV, it would first be high pass filtered with a 6th order Butterworth filter with 20 Hz cut off frequency. This processing step was necessary to remove low frequency noise and eliminate the baseline wandering effect [69]. The filter was applied again backwards to eliminate phase distortion. Then, the first and last 512 samples (250ms) were truncated to eliminate the artifact introduced by the filter at the edge. Then, the signal was transformed using Teager-Kaiser operation [67]:

$$y_i = x_i^2 - x_{i+1}x_{i-1} \tag{7}$$

This step amplified the movement onset signals significantly. Once the signal was rectified, it was passed through a median filter (256 samples for wrist movement detection electrodes and 512 samples for tongue movement detection electrodes, these numbers are determined empirically).

Then, the movement onset was determined for each motor task. For wrist extension movement, the differential signal between two electrodes were used for the preprocessing steps above to eliminate common noise. The movement onset was determined to be the first data point that has crossed the 12th standard deviation for 1024 samples. The threshold and hold period were determined empirically. For tongue protrusion movement, data from both electrodes were processed separately for the preprocessing steps above. The movement onset was determined to be the average of movement onset time from both

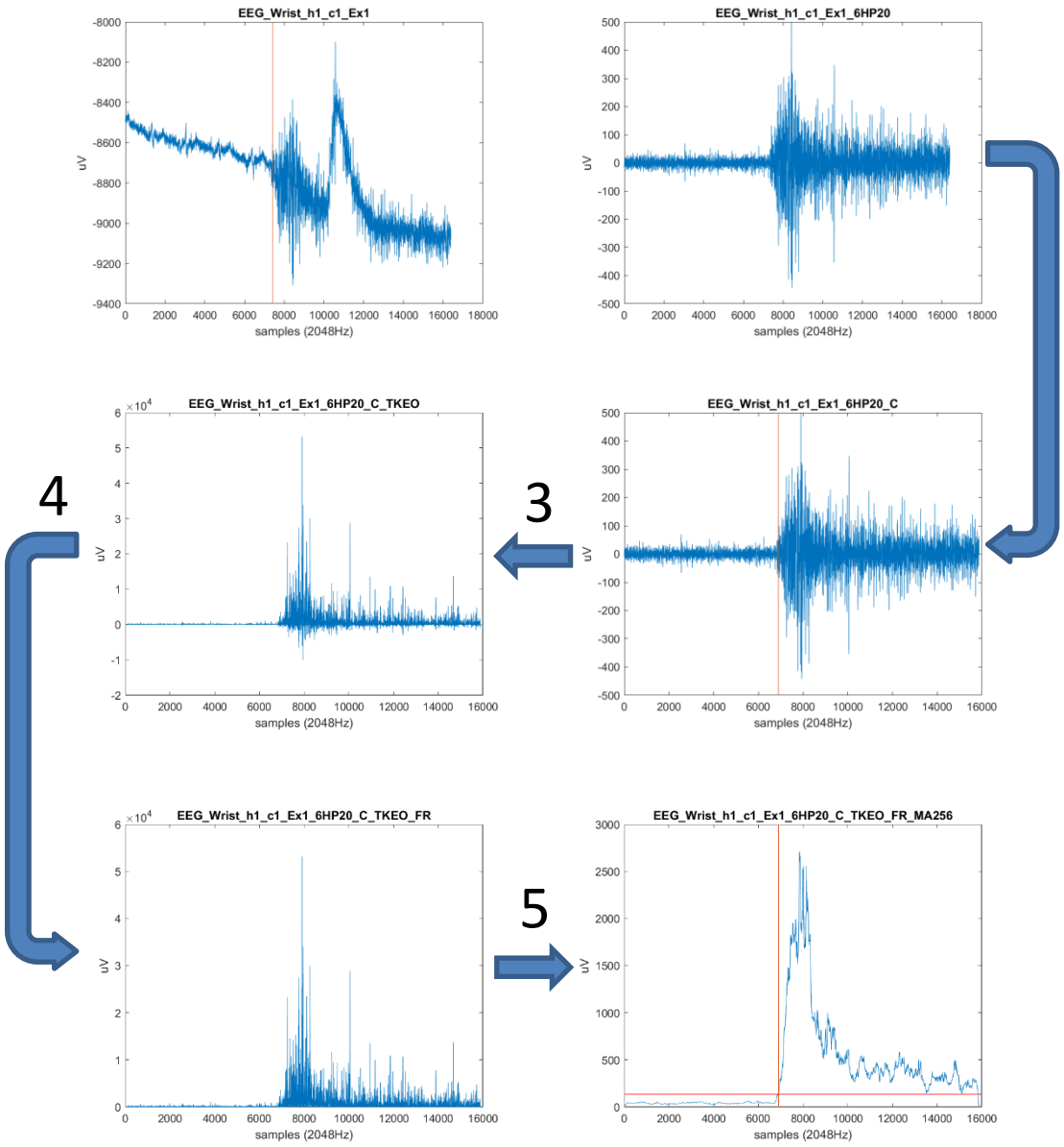

Figure 5.3 Example of wrist *EMG onset detection starting from differential signal (top left) with the following processing steps: 1.* 6th order Butterworth filter with cutoff frequency of 20Hz (use backward and forward filter to avoid phase distortion) 2. Cut of some samples in the beginning to avoid unwanted noise. 3. Perform Teager-Kaiser operation: $y(i)=x(i)\text{^}2-x(i+1)*x(i-1)$. Full wave rectification. 5. Median filter (256 samples for wrist and 512 samples for tongue). Use the first 2 seconds data as baseline and find the first data point that has crossed the 12th standard deviation for 1024 samples for wrist EMG data. (or the 4th standard deviation for 512 samples for tongue EMG data). The tongue EMG onset time is determined by the average of results from two electrodes.

electrodes. For each electrode, the movement onset was determined to be the first data point that has crossed the 4th standard deviation for 512 samples. The threshold and hold period were determined empirically. For concurrent initiation of the tongue protrusion and wrist extension, the movement onset was determined using the wrist extension movement. Finally, trials with unclear movement onset were excluded through visual inspection.

5.2.4 Event related desynchronization (ERD)

A series of steps were necessary to determine ERD using EEG and EMG data. Once the raw EEG data was extracted and converted to unit in uV, it was first resampled from 2048 Hz to 256 Hz to reduce processing time. Then, it was band pass filtered from 10 to 12 Hz using recommended filter option provided by EEGLAB [70]. Then, all EEG channels were referenced to the average of the following electrodes (F3, Fz, F4, C3, Cz, C4, P3, Pz, P4). Once the EEG signal was epoched based on the movement onset obtained in the previous step, the signal was then baselined to the data from -2.5 to -1.5 s to the movement onset. At this time, the researchers would visually inspect each epoch and remove any epochs that contains artifacts (eye blinking, electrode shifting etc.). The power of the passing epoch was averaged and fed through a moving average filter (32 samples which is determined empirically). Then, the degree of desynchronization around the movement onset was quantified by the power reduction of the sensorimotor area for the right arm electrode (C3) compared with the baseline (from -2.5 to -1.5 s in reference to the onset of movement) as shown in Figure 5.4.

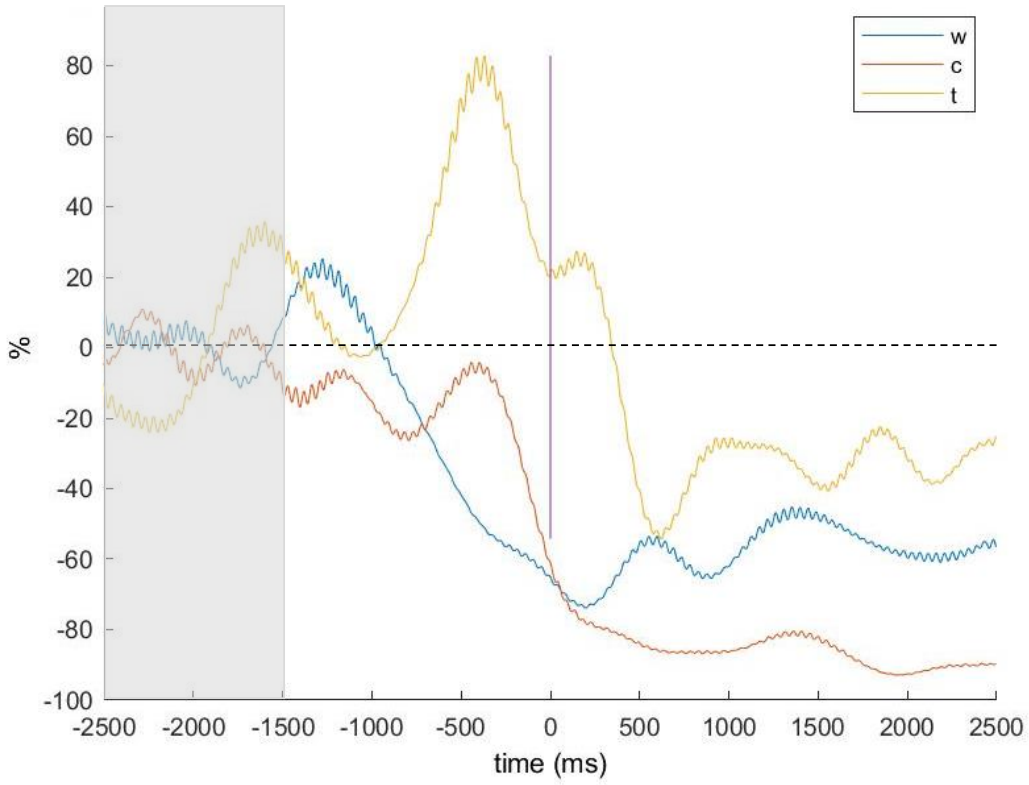

Figure 5.4 Example of event related potential change in EEG for tongue protrusion (t), wrist extension (w), and concurrent tongue protrusion and wrist extension (c) in 10-12 Hz compared with the baseline (from -2.5 to -1.5 s) across trials.

5.3 Results

The ERD for wrist extension (w), tongue protrusion (t), and concurrent tongue protrusion and wrist extension (c) for pre-movement (-1.5 to 0 s) and post-movement (0 to 2 s) is shown in Figure 5.5. Reductions in 10-12 Hz power around the movement onset were observed in all three tasks across subjects. On average, the largest reductions were observed around 0-1 s in reference to the movement onset. The greater reductions with the concurrent movement compared with the independent wrist or tongue movement were observed before and/or after the onset of movement in all subjects. When the reductions before the onset were summated, ERD during the concurrent wrist and tongue movement (26.8%) was greater than the wrist (21.2%) and tongue (2.7%) movement, on average.

Similarly, ERD after the onset (from 0 to 2.0 s) was greater during the concurrent movement (76.9%) than the wrist (62.7%) and tongue (29.0%) movement, on average.

5.4 Discussion and Conclusion

The preliminary observation of a tendency for a greater event-related desynchronization with concurrent tongue movement implies facilitation of brain excitability for limb movement, which may contribute to enhanced rehabilitation outcome in stroke survivors using TDS with motor rehabilitation. In conclusion, the preliminary results showed a tendency of a facilitatory effect of adding tongue movement to limb movement on event-related desynchronization in EEG, implying enhanced brain excitability.

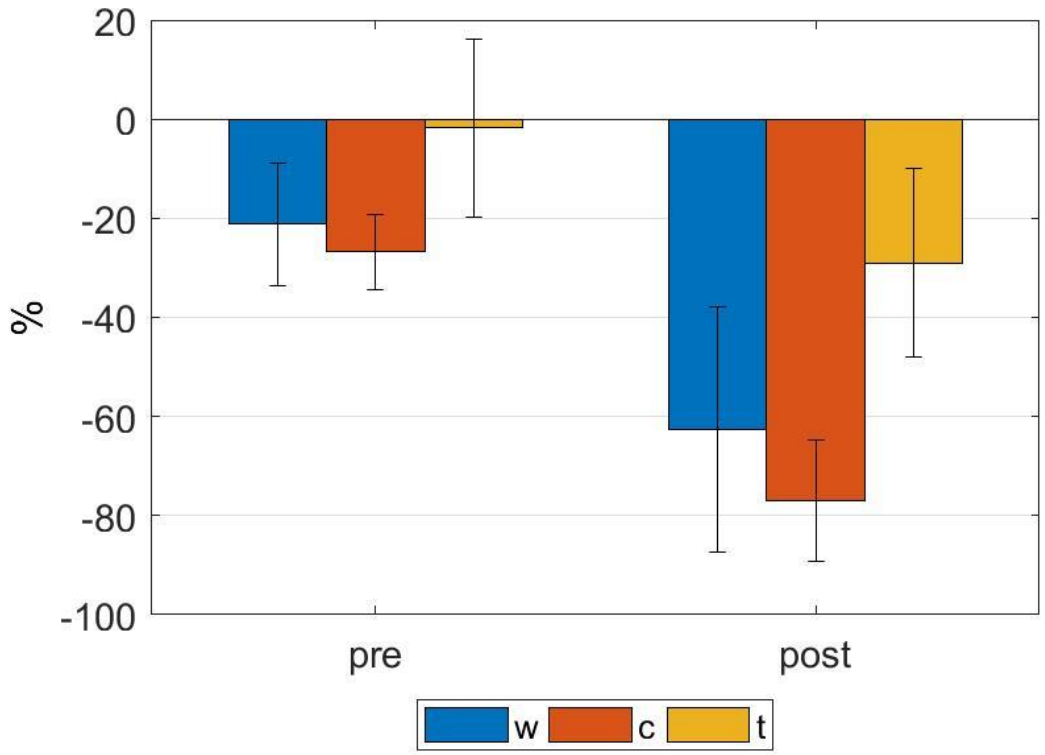

Figure 5.5 ERD for wrist extension (w), tongue protrusion (t), and concurrent tongue protrusion and wrist extension (c) for pre-movement (-1.5 to 0 s) and post-movement (0 to 2 s)

CHAPTER 6 CONCLUSION AND FUTURE WORK

6.1 Conclusion

Stroke is a devastating condition that may cause upper limb paralysis. Robotic rehabilitation with self-initiated and assisted movements is a promising technology that could help restore upper limb function. We have developed and evaluated a tongue-operated exoskeleton that will harness the intention of stroke survivors with upper limb paralysis via tongue motion to control robotic exoskeleton during rehabilitation to achieve functional restoration and improve quality of life. Specifically, a tongue operated assistive technology is called the Tongue Drive System is used to control rehabilitation robot such as wrist based exoskeleton Hand Mentor Pro^{TM} and upper limb based exoskeleton KINARM^{TM}.

Through a pilot trial from 3 healthy participants, we have demonstrated the functionality of an enhanced TDS-HM prototype that includes a BLE eTDS headset, HM Pro^{TM}, and a custom designed interface in the form of a USB dongle. The new TDS-HM has pressure-sensing capability that can add rehabilitation tasks based on isometric mode. The system can add a programmable load force to increase the exercise intensity in isotonic mode. A force protection mechanism was also added to reduce the risk of injury. The tongue-operated isotonic proportional control mode SSP algorithm was improved by adding PWM-based output to the HM motor.

Through a healthy subject experiment (7 males and 3 females, age 23-60 years) and a stroke subject experiment (age 32 and 58 years, Fugl-Meyer upper extremity baseline

score 35 and 13), we have demonstrated that the TDS-KINARM system could accurately translate tongue commands to exoskeleton arm movements, quantify function of the upper limb and perform rehabilitation training. Specifically, all healthy subjects and the stroke survivor successfully performed target reaching and tracking tasks in all control modes. One of the stroke patients shows clinically significant improvement.

We also found through a 10 healthy subject experiment that the PT mode is similar to A and AV modes compared to DT. This result indicates that the PT control strategy is a better candidate than the DT for the tongue assisted rehabilitation. This study also provides initial insights into possible kinematic similarities between tongue-operated and voluntary arm movements. Furthermore, the results show that the viscous resistance to arm motion does not affect kinematics of arm reaching movements significantly.

Finally, through a 6 healthy subject experiment, we observed a tendency of a facilitatory effect of adding tongue movement to limb movement on event-related desynchronization in EEG, implying enhanced brain excitability. This effect may contribute to enhanced rehabilitation outcome in stroke survivors using TDS with motor rehabilitation.

6.2 Future Work

6.2.1 Analysis of brain excitability at the onset of limb and tongue movement

A similar experiment similar in Chapter 5 was conducted. In this experiment, the wrist extension motion was replaced to elbow extension motion. In the future, we would

like to determine if similar faciliatory effect of adding tongue movement for event-related desynchronization in EEG holds for limb movement.

6.2.2 TDS-KINARM experiment with EEG and EMG recording

The experiment similar in Chapter 3 was conducted with 3 healthy participants for one 3-hour session and 1 stroke participant for six 3-hour sessions (the same stroke subject #2 in Chapter 3). In addition to KINARM and TDS, ActiveTwo^{TM} was added for EEG and EMG signal acquisition as shown in Figure 6.1.

During this experiment, we collected EEG signal in the motor cortex area and EMG signal for elbow and shoulder flexor and extensor as shown in Figure 6.2. In the future, we would like to evaluate the effect of tongue movement to brain activity while performing rehabilitation tasks.

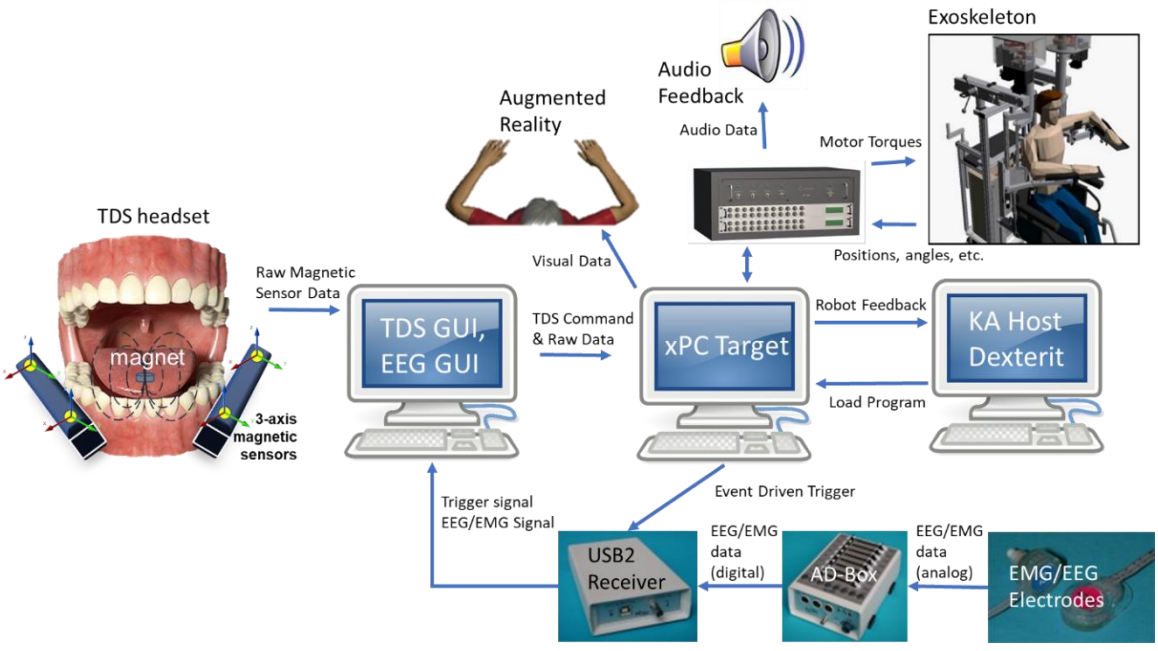

Figure 6.1 System Block Diagram for TDS-KINARM experiment with EEG and EMG recording.

(a) (b) (c)

Figure 6.2 TDS-KINARM experiment with EEG and EMG recording. (a) shows the participant sitting in KINARM wearing both EEG cap and TDS system. (b) shows the EMG electrode placement for elbow flexor and extensor. (c) shows the EMG electrode placement for shoulder extensor.

6.2.3 Improved Design and Evaluation of Tongue Drive System optimized for capturing precise tongue movement

Ideally, the Tongue Drive System should capture the precise kinematics of tongue movement. However, the currently existing TDS could only issue discrete or 1D proportional command. This is caused by the construction of the existing system. Specifically, all four magnetic sensors are in the same 2D plane with limited spacing between anterior and posterior direction.

An improved Tongue Drive System optimized for capturing precise tongue movement was developed (Figure 6.3). A laser printed structure made from medium-density fibreboard (MDF) with 3 mm thickness was constructed to hold the sensor in the location and orientation relative to the surface of the corner mark on the bottom right from user's perspective. The rough estimation can be found in Table 6.1. Adafruit Feature

Table 6.1 Approximate location and orientation of all magnet sensors. All sensor rotation procedure is using right hand rule. After applying rotation z, y, and x (order matters), the sensor will be in the same coordinate as the global coordinate as shown in Figure 6.4. The rotation angle is positive if the rotation is in the counter-clockwise direction when viewed by an observer looking along the y-axis towards the origin.

Name	x rotation (degree)	y rotation (degree)	z rotation (degree)	x pos (mm)	y pos (mm)	z pos (mm)
L1	0	90	180	97	50	35
L2	-90	0	90	75	-2	35
L3	-90	0	0	35	-2	75
R1	0	-90	180	-27	50	35
R2	-90	0	90	-5	-2	35
R3	-90	0	0	35	-2	05

nRF52840 Express board was used as part of the TDS hardware. This board provides hardware for both wired and wireless communication, Li battery power management, and sensor data acquisition via a star SPI configuration. An additional cape was designed to connect the nRF52840 board to the top sensor (LSM9DS1) and six sensors around user's cheek (LSM3MDLTR).

A 3D positioning system with 0.1mm accuracy was built based on Creality3D Ender-3 3D printer as shown in Figure 6.5. This device was used to develop and evaluate the Tongue Drive System by collecting magnet sensor data while precisely placing the magnet in different locations.

Magnetic sensor data was collected with magnet location from 5 to 65 mm in x axis, from 10 to 70 mm in y axis, and from 5 to 65 mm in z axis with 5 mm apart. Each position contained 50 data point.

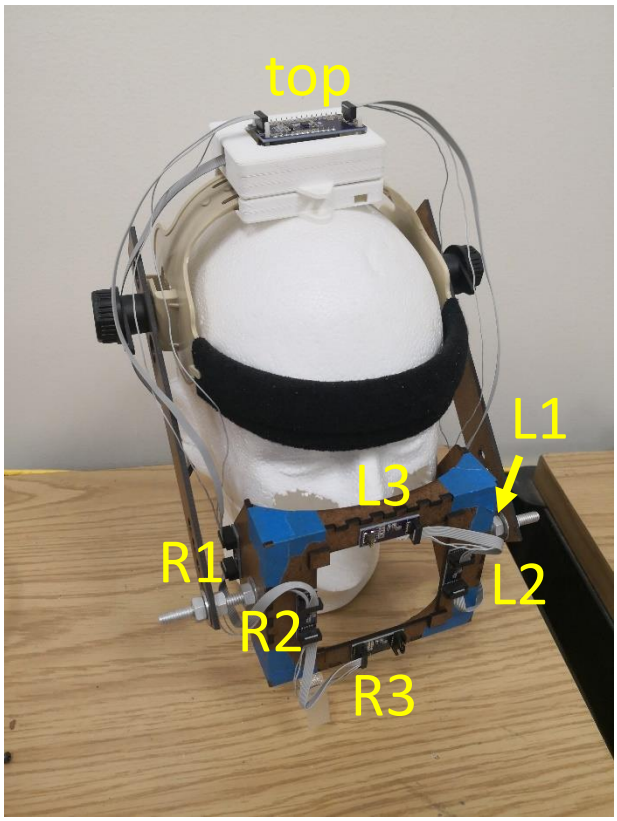

Figure 6.3 Enhanced Tongue Drive System Prototype.

A preliminary version of the enhanced algorithm based on [71] was developed. Instead of transforming the dipole model to raw magnetic sensor using different sensor parameters such as gain, offset, position, rotation, magnetic tracer's residual flux density, rotation, and EMF, the proposed method transforms the raw magnetic sensor data to the model. This will resolve issue in the previous method where certain sensor data has more weight than the others due to sensor parameter variation. In addition, the system could adapt to rotation with the addition of top sensor as long as the relative position among the sensors are fixed. The analysis is all done in the right-hand coordinate system.

Previous study has shown that the static magnetic flux density of a cylindrical magnet with thickness l, diameter d, and residual magnetic strength B_r at location $\boldsymbol{a} =$

$[a_x\ a_y\ a_z]$ with magnetic dipole moment pointed θ away from z axis and ϕ away from x axis measured at location $s = [s_x\ s_y\ s_z]$ can be expressed by the following:

$$B_{model} = \frac{\mu_0}{4\pi}\frac{3[\boldsymbol{m}\cdot(\boldsymbol{s}-\boldsymbol{a})](\boldsymbol{s}-\boldsymbol{a}) - \|\boldsymbol{s}-\boldsymbol{a}\|^2\boldsymbol{m}}{\|\boldsymbol{s}-\boldsymbol{a}\|^5} \tag{8}$$

where $\boldsymbol{m} = m\cdot[\sin(\theta)\cdot\cos(\phi), \sin(\theta)\cdot\sin(\phi), \cos(\theta)]$ is the magnetic moment vector of the dipole, and $m = \pi B_r d^2 l/(4\mu_0)$.

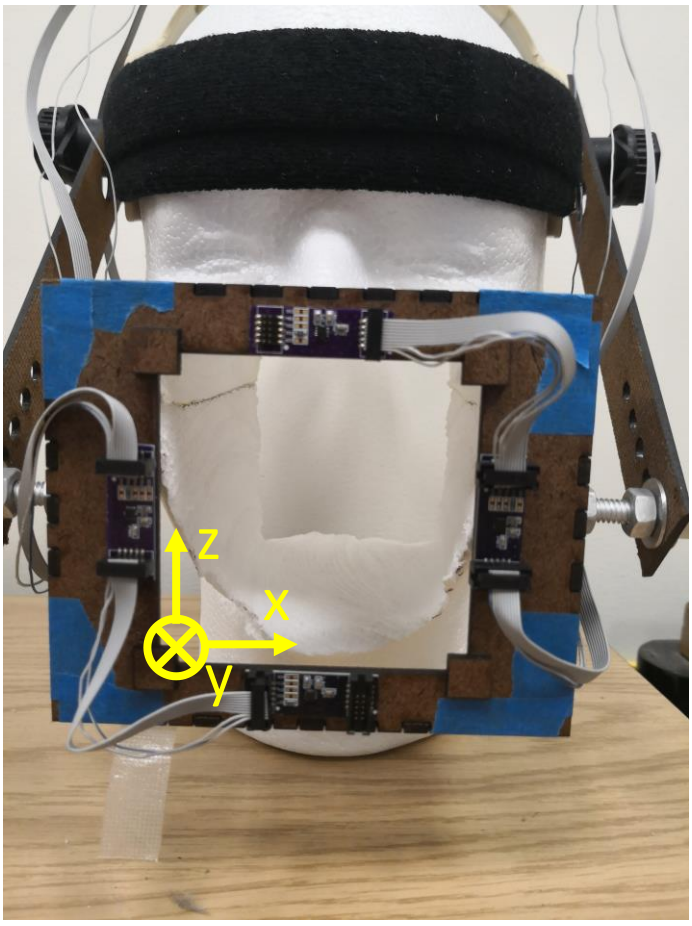

Figure 6.4 Orientation and location of all sensors are relative to the front surface of the alignment mark on the bottom right corner from user' perspective

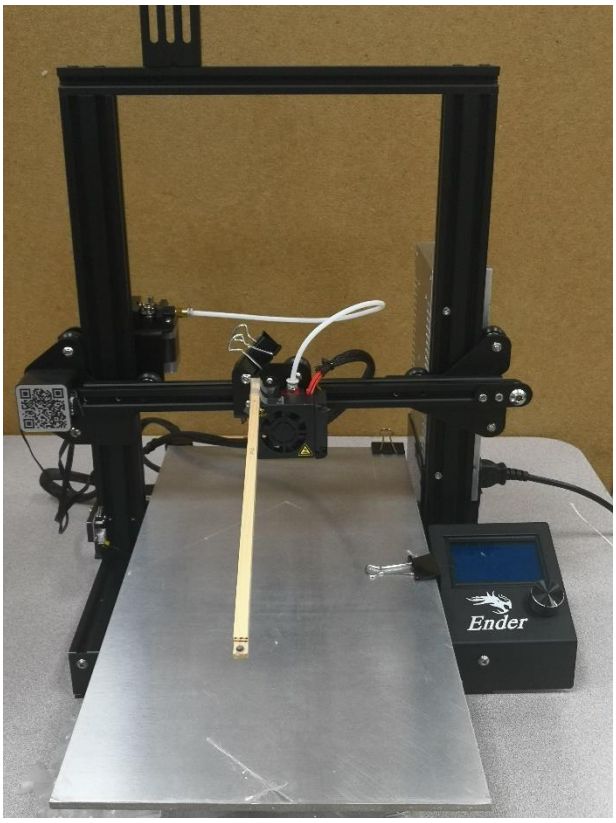

Figure 6.5 3D magnet positioning platform.

If the sensor is ideal, share the same coordinate system as the global coordination system, and there is no other magnetic field, we can estimate the location and orientation of the magnet if the sensor location is given by minimize the fitness function below using different optimization algorithms:

$$F = \frac{1}{n}\sum_{i=1}^{n} \|\boldsymbol{B}_i - \boldsymbol{B}_{model}\|^2 \tag{9}$$

where n is the total number of observation sensors.

In order to consider the practical issues, B_i can be expressed as

$$\boldsymbol{B}_i = \left[C\left(\boldsymbol{B}_{raw,i} - \boldsymbol{B}_{O,i}\right).* \boldsymbol{g}_i\right]\boldsymbol{R}_i - \boldsymbol{B}_{EMF}$$

where .∗ means element wise multiplication, C is a scalar that convert the digital reading from sensors to SI unit, $\boldsymbol{B}_{raw,i} = [B_{raw,i,x}\ B_{raw,i,y}\ B_{raw,i,z}]$ is the direct digital readings from sensor i, $\boldsymbol{B}_{0,i} = [B_{0,i,x}\ B_{0,i,y}\ B_{0,i,z}]$ is the sensor i reading offset in SI unit, $\boldsymbol{g}_i = [g_{i,x}\ g_{i,y}\ g_{i,z}]$ is the sensor I gain offset. $\boldsymbol{R}_i$ is the rotational matrix that transform the sensor i coordinate to global coordinate, and $\boldsymbol{B}_{EMF}$ is the external magnetic field in global coordinate system.

In order to utilize the system and predict the location and orientation of the magnet, we have approximated all parameters with known magnet location and orientation. Then, we could predict the magnet location and orientation by solving the optimization problem using the parameters obtained in the calibration step. In the future, we need to evaluate the system further with human subject trial.

APPENDIX A. LIST OF PUBLICATIONS

A.1 Journal Papers

- S. Ostadabbas, S. N. Housley, N. Sebkhi, K. Richards, D. Wu, **Z. Zhang**, M. G. Rodriguez, L. Warthen, C. Yarbrough, S. Balagaje, A. J. Butler, and M. Ghovanloo, "A Tongue-Controlled Robotic Rehabilitation: Preliminary Evidence for Function and Quality of Life Improvement in Stroke Survivors," *Journal of Rehabilitation Research & Development (JRRD)*, Jan. 2016.

A.2 Conference Papers

- **Z. Zhang**, S. Ostadabbas, M.N. Sahadat, N. Sebkhi, D. Wu, A.J. Butler, and M. Ghovanloo, "Enhancements of A Tongue-Operated Robotic Rehabilitation System," Proc. IEEE Biomedical Circuits and Systems Conf., Atlanta, GA, 2015, pp. 25-28.
- M. Ghovanloo, M.N. Sahadat, **Z. Zhang**, F. Kong, and N. Sebkhi, "Tapping into tongue motion to substitute or augment upper limbs," *SPIE*, Anaheim, California, USA, May 18, 2017.
- **Z. Zhang**, B. Prilutsky, M. Shinohara, A. Butler, and M. Ghovanloo, "Preliminary Evaluation of a Tongue-Operated Exoskeleton for Post-Stroke Upper Limb Rehabilitation," *Archives of Physical Medicine and Rehabilitation*, vol. 98, no. 12, e163, 2017.
- F.J. Chu, R. Xu, **Z. Zhang**, P.A. Vela, M. Ghovanloo, "The Helping Hand: An Assistive Manipulation Framework Using Augmented Reality and Tongue-Dirve Interfaces," *EMBC2018*, Honolulu, HI, USA, July 18-21, 2018, pp. 2158-2161.
- F.J. Chu, R. Xu, **Z. Zhang**, P.A. Vela, and M. Ghovanloo, "The Helping Hand: An Assistive Manipulation Framework Using Augmented Reality and a Tongue Drive," arXiv preprint arXiv: 1802.00463.
- F.J. Chu, R. Xu, **Z. Zhang**, P.A. Vela, M. Ghovanloo, "Hands-Free Assistive Manipulator Using Augmented Reality and Tongue Drive System," IROS2018, Oct. 1-5, 2018, pp. 5463-5468,
- **Z. Zhang**, E. Seraj, K. Mahalingam, B.I. Prilutsky, M. Shinohara, A. Butler, and M. Ghovanloo, "A Tongue-Operated Upper Extremity Robotic System for Stroke Rehabilitation," Transnational Research in Stroke Initiative (TRSI), Atlanta, USA, Sept. 22, 2018.
- A.J. Butler, M.A. Al-Ganim, A.J. Edenfield, **Z. Zhang**, B.I. Prilutsky, M. Ghovanloo, "Can the use of a tongue-driven robot improve upper extremity impairmentin patients with stroke" PTAG, Atlanta, GA, USA, Mar. 21-24, 2019.
- **Z. Zhang,** J. Strunk, and M. Shinohara, "Brain excitability at the onset of voluntary wrist movement can be enhanced with concurrent tongue movement," ISEK, Virtual, July 12-14, 2020.
- **Z. Zhang,** M. Ghovanloo, M. Shinohara, A. Butler, and B. I. Prilutsky, "Arm reaching controlled by a tongue-operated exoskeleton system: Implications for stroke rehabilitation," ASB, Virtual, August 4-7, 2020.

APPENDIX B. TONGUE DRIVE SYSTEM DEVELOPMENT

B.1 Bluetooth based TDS design for KINARM interface

Multiple enhancements were made on TDS to obtain better performance and reliability for KINARM interface described in Chapter 3. The updated headset contains two magnetic sensor modules, a control module, a Li-ion battery, a commercially available headgear, two 3D printed arms that provide support for magnetic sensors, and one 3D printed box that stores the battery and control module. Each magnetic sensor module contains two magnetic sensors (LSM303D, ST) that are 3.1 cm apart from each other. The control module contains the Bluetooth low energy (BLE) wireless MCU (CC2541, TI), a magnetic sensor (LSM9DS1, ST), Li-ion battery charging circuits (LTS4054, ADI), power management circuits (TPS71733, PS61220, TI), a switch, and all the supporting circuitry for the components above. An nRF52 based TDS headset was also developed with additional wired connectivity.

After the headset is turned on, the MCU performs a self-check routine to ensure that all the sensors are functional. Then, it initializes all the sensors to have dynamic range of ±8 gauss and sampling rate of 100 Hz for LSM303D and 80 Hz for LSM9DS1. Subsequently, it starts advertising indefinitely after setting up custom designed BLE service and characteristics. After connecting to USB dongle, the headset either enters active mode or sleep mode. In the active mode, all data are transferred to eTDS's MCU via serial peripheral interface bus (SPI), and then to a receiver dongle via BLE, and to PC via UART serial communication at 50 Hz. The PC processes the raw magnetic sensor data to either

discrete commands or 1D continuous command. In the sleep mode, all the sensors are put to sleep, and the headset maintains connectivity with the receiver dongle.

A LabVIEW based GUI was developed to control the receiver dongle to establish/terminate BLE wireless connection based on headset's MCU MAC address. The GUI can also switch the headset between sleep and active mode.

Several sub GUIs were developed to convert the raw magnetic sensor data to commands for KINARM^{TM}. These sub GUIs visualize and store raw magnetic sensor data, perform earth magnetic field (EMF) cancellation, train the pattern recognition algorithm to map tongue gestures to either five discrete commands or one-dimensional continuous command, as well as perform the classification in real time and feed the results to KINARM^{TM} via RS-232 serial communication (Figure 0.1).

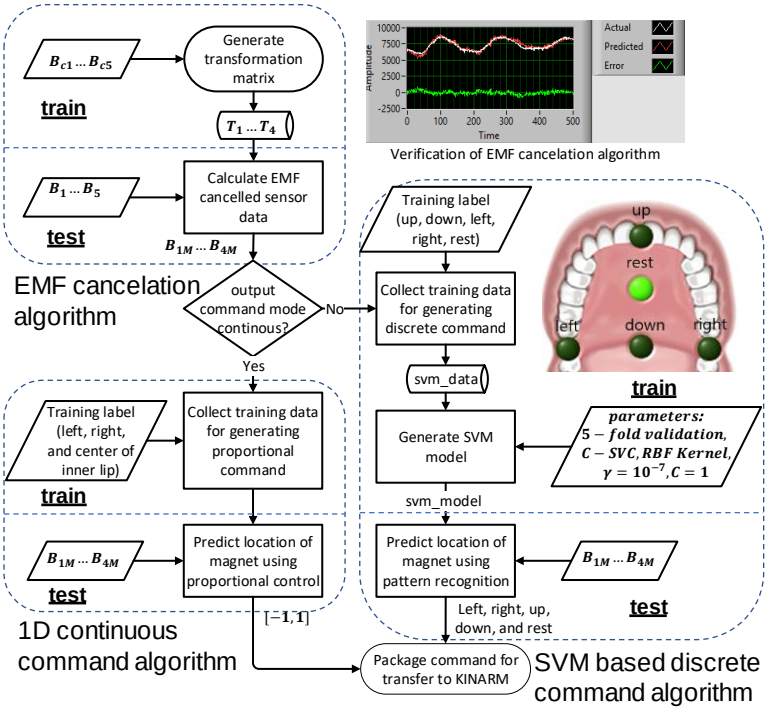

Figure 0.1 Flow Chart for TDS sensory signal processing algorithm.

Ideally, the magnetic sensor should sense only the magnetic flux density from the magnet attached in the tongue (between 0.1 and 8 gauss). However, the magnetic sensor also senses signals from other sources such as the earth magnetic field (0.25 to 0.65 gauss). The performance of the TDS would decrease without an effective preprocessing algorithm that removes or reduces irrelevant magnetic signals. We have developed a preprocessing algorithm to eliminate the effect of the unwanted magnetic fields.

The magnetic flux density sensed by each sensor in the sensor module ($\boldsymbol{B_1}, \dots, \boldsymbol{B_4} \in \mathbb{R}_{\boldsymbol{n\times 3}}$) is from both the unwanted magnetic field ($\boldsymbol{B_{1E}}, \dots, \boldsymbol{B_{4E}} \in \mathbb{R}_{\boldsymbol{n\times 3}}$) and the desired magnetic field ($\boldsymbol{B_{1M}}, \dots, \boldsymbol{B_{4M}} \in \mathbb{R}_{\boldsymbol{n\times 3}}$), where

$$\begin{aligned} \boldsymbol{B_1} &= \boldsymbol{B_{1E}} + \boldsymbol{B_{1M}} \\ &\dots \\ \boldsymbol{B_4} &= \boldsymbol{B_{4E}} + \boldsymbol{B_{4M}} \end{aligned} \tag{10}$$

In the EMF cancelation sub GUI, $n = 500$ samples are collected while asking the participant to keep their tongue still in resting position in the center of the mouth and to rotate his/her head around. Since the relative position between the magnet and each sensor are more than 5 cm in the above data collection method, $\boldsymbol{B_{1M}}, \dots, \boldsymbol{B_{4M}}$ are relatively small (<0.1 gauss). Ideally however, this step should be done without magnet attached in the tongue. We can approximate the magnetic flux density sensed by the sensors in the sensor module in the calibration stage ($\boldsymbol{B_{C1}}, \dots, \boldsymbol{B_{C4}}$) as

$$\begin{aligned} \boldsymbol{B_{C1}} &\approx \boldsymbol{B_{1E}} \\ &\dots \\ \boldsymbol{B_{C4}} &\approx \boldsymbol{B_{4E}} \end{aligned} \tag{11}$$

The magnetic field exerted to the sensors in the control module ($\boldsymbol{B_5} \in \mathbb{R}_{\boldsymbol{n\times 3}}$) contains mainly the EMF component ($\boldsymbol{B_{5E}} \in \mathbb{R}_{\boldsymbol{n\times 3}}$) because it is far away (>20 cm) from the desired magnetic field.

$$\boldsymbol{B_5 = B_{C5} = B_{5E}} \tag{12}$$

Unlike the magnetic field from the magnet attached to the tongue, the magnitude of most unwanted magnetic fields exerts the same magnetic flux density to the sensors.

$$\|\boldsymbol{B_{1E}}\| = \|\boldsymbol{B_{2E}}\| = \|\boldsymbol{B_{3E}}\| = \|\boldsymbol{B_{4E}}\| = \|\boldsymbol{B_{5E}}\| \tag{13}$$

Thus, we can use these samples to find the transformation matrix ($\boldsymbol{T_1, T_2, T_3, T_4} \in \mathbb{R}_{4\times 3}$) to map magnetic flux density sensed by the sensors from the control module ($\boldsymbol{B_{C5}} \in \mathbb{R}_{n\times 3}$) to each sensor from the sensor module ($\boldsymbol{B_{C1}, B_{C2}, B_{C3}, B_{C4}} \in \mathbb{R}_{n\times 3}$).

$$\begin{gathered}\boldsymbol{T_1} = \left[\boldsymbol{J_{n,1}}\ \boldsymbol{B_{C5}}\right]^{-1}\boldsymbol{B_{C1}} \\ \ldots \\ \boldsymbol{T_4} = \left[\boldsymbol{J_{n,1}}\ \boldsymbol{B_{C5}}\right]^{-1}\boldsymbol{B_{C4}}\end{gathered} \tag{14}$$

$\boldsymbol{J_{n,1}}$ is a vector of 1s with n rows and 1 column.

After finding the transformation matrix $\boldsymbol{T_1} \ldots \boldsymbol{T_4}$, we can find magnetic flux density without the earth magnetic field:

$$\begin{gathered}\boldsymbol{B_{1M} = B_1 - B_{1E} \approx B_1 - B_{C1} \approx B_1 - \left[J_{n,1}\ B_{C5}\right]T_1 \approx B_1 - \left[J_{n,1}\ B_5\right]T_1} \\ \ldots\end{gathered} \tag{15}$$

$$\boldsymbol{B_{4M} = B_4 - B_{4E} \approx B_4 - B_{C4} \approx B_4 - \left[J_{n,1}\, B_{C5}\right] T_4 \approx B_4 - \left[J_{n,1}\, B_5\right] T_4}$$

Several algorithms have been developed to translate magnetic sensor data to discrete commands. Support vector machine (SVM) with radial basis function (RBF) kernel performs the best [72]. We have developed the discrete command pattern recognition algorithm based on LabVIEW LIBSVM library [73].

In the training sub GUI, users associate their tongue position to each command (up, down, left, right, and rest) three times in random order. A total of $n = 50$ sample points of magnetic sensor data needs to be recorded for each tongue position and repetition. Then, a model is generated with $\gamma = 10^{-7}, C = 1$ with 5-fold validation where γ controls the weight of training sample and C controls the amount of regularization for the model. To reduce the effect of speech accidentally triggering the command, the operator instructs the users to associate the location of the tongue command to places that are generally not used for speech. Further, sensor data are recorded while instructing the users to speak briefly (500 samples). These data are included in the model as the rest command.

In the predicting sub SUI, the algorithm performs classification using 10 past EMF cancelled data. If all the classification results are the same, the command to KINARM™ will be updated.

The 1D continuous command algorithm translates the raw magnetic sensor data to a continuous number between -1 and 1 to indicate the position of the tongue between left most and right most positions.

In the training sub GUI, $n = 50$ samples are collected for three tongue positions each (left, center, right). Then, we calculate and record the mean magnitude of the EMF cancelled front magnetic sensor (sensor 1) in the left sensor module when tongue is on the left corner of the inner lip ($\|\boldsymbol{B_{cl}}\|$), and front magnetic sensor in the right sensor module (sensor 3) when tongue is on the right corner of the inner lip ($\|\boldsymbol{B_{cr}}\|$). In the predicting sub GUI, the algorithm outputs are obtained every 10 ms based on the average results of past $m = 10$ samples. Specifically, it first calculates the magnitude of the EMF cancelled left front ($\|\boldsymbol{B_l}\|$) and right front sensors ($\|\boldsymbol{B_r}\|$). If $\|\boldsymbol{B_l}\| > \|\boldsymbol{B_r}\|$, scaling factor S would be set to $\|\boldsymbol{B_{cl}}\|$. Otherwise, $S = ||\boldsymbol{B_{cr}}||$. Each individual result is calculated with the following equation:

$$Result = sign(\|\boldsymbol{B_l}\| - \|\boldsymbol{B_r}\|) * \left(\frac{abs(\|\boldsymbol{B_l}\| - \|\boldsymbol{B_r}\|)}{S}\right)^{\frac{1}{2}}$$

B.2 Initial development of embedded algorithm for Tongue Drive System

A preliminary prototype as shown in Figure 0.2 is developed to move all the sensory signal processing algorithm in the TDS used for KA system on the embedded system. Mbed LPC1768 Development Board was used as the main embedded processor. A microSD reader and microSD card were used to store necessary training data and generated SVM model. Four LSM303D Breakout Board were used to sense magnetic flux. All components were built in a breadboard as shown in Figure 0.3. A customized C# based GUI was also developed to control the prototype from PC. A request-response Serial library from the ARM® Mbed™ IoT Device Platform was used to communicate with PC. This study shows that it is feasible to run sensory signal processing algorithm with microcontroller. However,

only limited training data could be collected, and the EMF cancelation algorithm was not included because the matrix inversion operation is not supported. A more capable microcontroller such as nRF52 could solve this problem with large on-board flash memory and floating-point computation capability.

B.3 Design of Assistive Manipulation Framework Using Augmented Reality and Tongue Drive System

TDS can also be used for collaborative manipulation task for person with physical disabilities. Specifically, the system consists of Tongue Drive System, a 7 DoF robotic arm, and an augmented reality interface. The system interprets user's environment and provide context based visual feedback to the augmented reality interface. The Bluetooth based TDS design for KA interface provides user input for triggering the robotic arm to execute the selected manipulation task from the augmented reality interface [74]. In this case, the tongue command is relayed to the robot by constantly updating a shared text document with the most updated command.

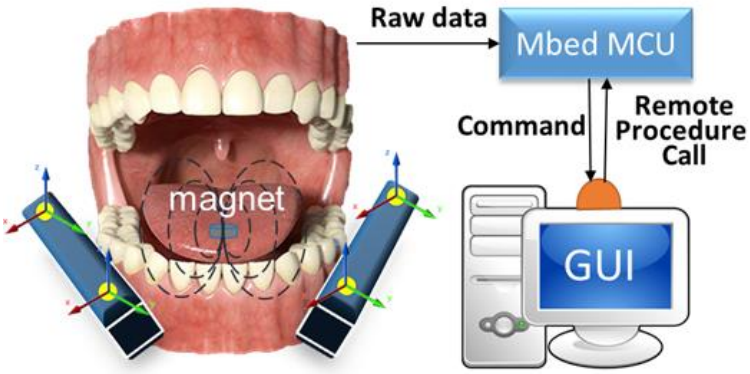

Figure 0.2 System Block Diagram of TDS with sensory signal processing algorithm in Mbed MCU.

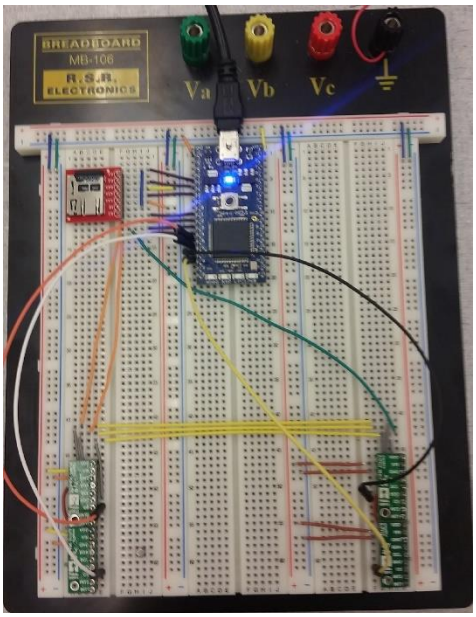

Figure 0.3 Setup of TDS with sensory signal processing algorithm in Mbed™ MCU.

REFERENCES

[1] E.J. Benjamin *et al.*, "Heart Disease and Stroke Statistics – 2017 Update," *Circulation*, vol. 136. No. 8, e229-e277, Mar. 2017.

[2] H. Nakayama, H. S. JØrgensen, H. O. Raaschou, T. S. Olsen, "Recovery of Upper Extremity Function in Stroke Patients: The Copenhagen Stroke Study," *Arch. Phys. Med. Rehabil.*, vol. 75, no. 4, pp. 394-398, Apr. 1994.

[3] N. Foley *et al.*, (2016, September). Evidence-Based Review of Stroke Rehabilitation, Chapter 10: Upper Extremity Interventions [Online]. Available: http://www.ebrsr.com/evidence-review/10-upper-extremity-interventions

[4] R.W. Teasell, N.C. Foley, S.K. Bhogal, M.R. Speechley, "An evidence-based review of stroke rehabilitation," *Topics in Stroke Rehabilitation*, vol. 10, no. 1, pp. 29-58, 2003.

[5] H.I. Krebs and N. Hogan, "Robotic therapy: the tipping point," *American Journal of Physical Medicine & Rehabilitation*, 91 (11 Suppl 3): S290-7, Nov. 2012.

[6] P. S. Lum, C. G. Burgar, P. C. Shor, M. Majmundar, and M. V. Loos, "Robot-assisted movement training compared with conventional therapy techniques for the rehabilitation of upper-limb motor function after stroke," *Archives of Physical medicine and Rehabilitation*, vol. 83, no. 7, pp. 952-959, Jul. 2002.

[7] G.B. Prange, M.J. Jannink, C.G. Groothuis-Ousdshoorn, H.J. Hermens, and M.J. Ijzerman, "Systematic review of the effect of robot-aided therapy on recovery of the hemiparetic arm after stroke, *J. Rehabil. Res. Dev.*, vol. 43, no. 2, pp. 171-184, Mar. 2006.

[8] J. Mehrholz, M. Pohl, T. Platz, J. Kugler, and B. Elsner, "Electromechanical and robot-assisted arm training for improving activities of daily living, arm function, and arm muscle strength after stroke," *Cochrane Database Syst Rev*, vol. 11, no. cd006876, Nov. 2015.

[9] D. Lynch, M. Ferraro, J. Krol, C.M. Trudell, P. Christos, B.T. Volpe, "Continuous passive motion improves shoulder joint integrity following stroke," *Clinical Rehabilitation*, vol. 19, no. 6, pp. 594-599, 2005.

[10] N. Hogan, H.I. Krebs, B. Rohrer, J.J. Palazzolo, L. Dipietro, S.E. Fasoli, J. Stein, R. Hughes, W. R. Frontera, D. Lynch, and B.T. Volpe, "Motions or muscles? Some behavioral factors underlying robotic assistance of motor recovery," *Journal of Rehabilitation Research & Development*, vol. 43, no. 5, pp. 605-618, Aug. 2006.

[11] M. Ferraro, J.J. Palazzolo, J. Krol, H.I. Krebs, N. Hogan, B.T. Volpe, "Robot-aided sensorimotor arm training improves outcome in patients with chronic stroke," *Neurology*, vol. 61, no. 11, pp. 1604-1607, 2003.

[12] M.A. Dimyan and L.G. Cohen, "Neuroplasticity in the context of motor rehabilitation after stroke," *Nature Reviews, Neurology*, vol. 7, no. 2, pp. 76-85, Feb. 2011.

[13] R.J. Nudo, B.M. Wise, F. SiFuentes, and G.W. Milliken, "Neural Substrates for the Effects of Rehabilitative Training on Motor Recovery After Ischemic Infarct," *Science*, vol. 272, pp.1791-1794, Jun. 1996.

[14] H.I. Krebs, V. Volpe, and N. Hogan, "A working model of stroke recovery from rehabilitation robotics practitioners," *Journal of NeuroEngineering and Rehabilitation*, Feb. 2009.

[15] A.A. Blank, J.A. French, A.U. Pehlivan, and M.K. O'Malley, "Current Trends in Robot Assisted Upper-Limb Stroke Rehabilitation: Promoting Patient Engagement in Therapy," *Curr. Phys. Med. Rehabil. Rep.*, vol. 2, no. 3, pp. 184-195, Sept. 2014.

[16] J.H. Morris, W.F. van, S. Joice, S.A. Ogston, I. Cole, and R.S. MacWalter, "A comparison of bilateral and unilateral upper-limb task training in early poststroke rehabilitation: a randomized control trial," *Archives of Physical Medicine Rehabilitation*, vol. 89, no. 7, pp. 1237-1245, Jul. 2008.

[17] F. Coupar, A. Pollock, F. van Wijck, J. Morris, and P. Langhorne, "Simultaneous bilateral training for improving arm function after stroke," *Cochrane Database Syst.* Rev. (4): CD006432, Apr. 2010.

[18] B. Cesqui, P. Tropea, S. Micera, and H.I. Krebs, "EMG-based pattern recognition approach in post stroke robot-aided rehabilitation: a feasibility study," *Journal of NeuroEngineering and Rehabilitation*, vol. 10, no. 75, Jul. 2013.

[19] A. Ramos-Murguialday, D. Broetz, M. Rea, L. Läer, O. Yilmaz, F.L. Brasil, G. Liberati, M.R. Curado, E. Garcia-Cossio, A. Vyziotis, W. Cho, M. Agostini, E. Soares, S. Soekadar, A. Caria, L.G. Cohen, N. Birbaumer, "Brain-machine interface in chronic stroke rehabilitation: a controlled study," *Annals of Neurology*, vol. 74, no. 1, pp. 100-108, Jul. 2013.

[20] J.L. Sullivan, N.A. Bhagat, N. Yozbatiran, R. Paranjape, C.G. Losey, R.G. Grossman, J.L. Contreras-Vidal, G.E. Francisco, and M.K. O'Malley, "Improving Robotic Stroke Rehabilitation by Incorporating Neural Intent Detection: Preliminary Results from a Clinical Trial," *2017 International Conference on Rehabilitation Robotics*, pp. 122-127, Jul. 2017.

[21] E. Niedermeyer, and F.L. da Silva, Eds., *Electroencephalography: basic principles, clinical applications, and related field*s, Philadelphia, Pennsylvania: Lippincott Williams & Wilkins, 2005.

[22] D. Novak and R. Riener, "Enhancing patient freedom in rehabilitation robotics using gaze-based intention detection*," IEEE Int. Conf. Rehabil. Robot*, Jun. 2013.

[23] J. Kim, C. Bulach, K.M. Richards, D. Wu, A.J. Butler, and M. Ghovanloo, "An Apparatuss for improving upper limb function by engaging synchronous tongue motion," *Proc. IEEE Neural Eng. Conf.*, pp. 1574-1577, Nov. 2013.

[24] S. Ostadabbas, S. N. Housley, N. Sebkhi, K. Richards, D. Wu, Z. Zhang, M. G. Rodriguez, L. Warthen, C. Yarbrough, S. Balagaje, A. J. Butler, and M. Ghovanloo, "A Tongue-Controlled Robotic Rehabilitation: Preliminary Evidence for Function and Quality of Life Improvement in Stroke Survivors," *Journal of Rehabilitation Research & Development (JRRD)*, Jan. 2016.

[25] E. Kandel, T. Jessel, J. Schwartz, S. Siegelbaum, and A. Hudsepeth, *Principles of Neural Science*, 5th ed., McGraw-Hill Education, 2012.

[26] Y. Danilov, K. Kaczmarek, K. Skinner, and M. Tyler, "Cranial Nerve Noninvasive Neuromodulation: New Approach to Neurorehabilitation," *Frontiers in Neuroengineering*, Chapter 44, 2015.

[27] R.D. Kent, "The uniqueness of speech among motor systems," *Clin. Linguit Phon.* vol. 18, no. 6-8, pp. 495-505, 2004.

[28] T. Uapathi, N. Venketasubramanian, K.J. Leck, C.B. Tan, W.L. Lee, H. Tjia, "Tongue deviation in acute ischaemic stroke: a study of supranuclear twelfth cranial nerve palsy in 300 stroke patients," *Cerebrovasc Dis.* vol. 10, no. 6, pp. 462-465, 2000.

[29] D.J. Mikulis, M.T. Jurkiewicz, W.E. Mcllroy, W.R. Staines, L. Rickards, S. Kalsi-Ryan, A.P. Crawley, M.G. Fehlings, and M.C. Verrier, "Adaptation in the motor cortex following cervical spinal cord injury," *Neurology*, vol. 58, no. 5, pp. 794-801, March 2002.

[30] M. Funk, K. Lutz, S. Hotz-Boendermaker, M. Roos, P. Summer, P. Brugger, M.-C. Hepp-Reymond, and S.S. Kollias, "Sensorimotor tongue representation in individuals with unilateral upper limb amelia," *NeuroImage*, vol. 43, no. 1, pp. 121-127, Oct. 2008.

[31] X. Huo, J. Wang, and M. Ghovanloo, "A Magneto-inductive sensor based wireless tongue-computer interface," *IEEE Trans Neural Systems and Rehab. Eng.*, vol. 16, no. 5, pp. 497-504, 2008.

[32] E. Sadeghian, X. Huo, and M. Ghovanloo, "Command detection and classification in tongue drive assistive technology," *Proc. IEEE Eng. in Medicine and Biology Society*, pp. 5465-5468, 2011.

[33] J. Kim et al., "The Computer and Wheelchair Control for People with Spinal Cord Injury," *Sci Transl Med*, vol. 5, no. 213, p. 213ra166, Nov. 2013, doi: 10.1126/scitranslmed.3006296.

[34] J. Harris and J. Eng, "Strength Training Improves Upper-Limb Function in Individuals with Stroke," *Stroke*, [Online]. Available: https://stroke.ahajournals.org/content/41/1/136.full#ref-list-1, 2009.

[35] X. Huo and M. Ghovanloo, "Evaluation of a wireless wearable tongue–computer interface by individuals with high-level spinal cord injuries," *J Neural Eng*, vol. 7, no. 2, p. 26008, Apr. 2010, doi: 10.1088/1741-2560/7/2/026008.

[36] X. Huo and M. Ghovanloo, "Tongue drive: a wireless tongue- operated means for people with severe disabilities to communicate their intentions," *IEEE Communications Magazine*, vol. 50, no. 10, pp. 128–135, Oct. 2012, doi: 10.1109/MCOM.2012.6316786.

[37] Z. Zhang, S. Ostadabbas, M.N. Sahadat, N. Sebkhi, D. Wu, A.J. Butler, and M. Ghovanloo, "Enhancements of A Tongue-Operated Robotic Rehabilitation System," *Proc. IEEE Biomedical Circuits and Systems Conf.*, Atlanta, GA, 2015, pp. 25-28.

[38] S. Ostadabbas et al., "Tongue-controlled robotic rehabilitation: A feasibility study in people with stroke," *J Rehabil Res Dev*, vol. 53, no. 6, pp. 989–1006, 2016, doi: 10.1682/JRRD.2015.06.0122.

[39] S.N. Housely, D. Wu, K. Richards, S. Belagaje, M. Ghovanloo, and A.J. Butler, "Improving Upper Extremity Function and Quality of Life with a Tongue Driven Exoskeleton: A Pilot Study Quantifying Stroke Rehabilitation," *Stroke Research and Treatment*, pp.13, 2017.

[40] N. Nordin, S.Q. Xie, and B. Wünsche, "Assessment of movement quality in robot-assisted upper limb rehabilitation after stroke: a review," *Journal of Neuroeng. Rehabil.*, vol. 11, no. 137, Sept. 2014.

[41] P. Maciejasz, J. Eschweiler, K. Gerlach-Hahn, A. Jansen-Troy, and S. Leonhardt, "A survey on robotic devices for upper limb rehabilitation," *Journal of Neuroeng. Rehabil.*, vol. 11, no. 3, Jan. 2014.

[42] S. Scott, "Apparatus for measuring and perturbing shoulder and elbow joint positions and torques during reaching," *Journal of Neuroscience Methods*, vol. 89, no. 2, pp. 119-127, Jul. 1999.

[43] S.P. Dukelow, T.M. Herter, S.D. Bagg, and S.H. Scott, “The independence of deficits in position sense and visually guided reaching following stroke,” *Journal of Neuroeng. Rehabil.*, vol. 9, no. 72, Oct. 2012.

[44] J. Kim, X. Huo, J. Minocha, J. Holbrook, A. Laumann, and M. Ghovanloo, “Evaluation of a Smartphone Platform as a Wireless Interface Between Tongue Drive System and Electric-Powered Wheelchairs,” *IEEE Transactions on Biomedical Engineering*, vol. 59, no. 6, pp. 1787–1796, Jun. 2012, doi: 10.1109/TBME.2012.2194713.

[45] P.M. Fitts and J.R. Peterson, “Information Capacity of Discrete Motor Responses,” *Journal of Experimental Psychology*, vol. 67, no. 2, pp. 103-112, Feb. 1964.

[46] I. S. MacKenzie, “Fitts’ law as a research and design tool in human-computer interaction,” *Hum.-Comput. Interact.*, vol. 7, no. 1, pp. 91–139, Mar. 1992, doi: 10.1207/s15327051hci0701_3.

[47] S. G. Hart and L. E. Staveland, “Development of NASA-TLX (Task Load Index): Results of Empirical and Theoretical Research,” in *Advances in Psychology*, vol. 52, P. A. Hancock and N. Meshkati, Eds. North-Holland, 1988, pp. 139–183.

[48] A.R. Fugl-Meyer, L. Jääskö, I. Leyman, S. Olsson, and S. Steglind, “The post-stroke hemiplegic patient. 1. a method for evaluation of physical performance,” *Scandinavian Journal of Rehabilitation Medicine*, vol. 7, no. 1, pp. 13-31, Jan. 1975.

[49] S. J. Page, G. D. Fulk, and P. Boyne, “Clinically Important Differences for the Upper-Extremity Fugl-Meyer Scale in People With Minimal to Moderate Impairment Due to Chronic Stroke,” *Phys Ther*, vol. 92, no. 6, pp. 791–798, Jun. 2012, doi: 10.2522/ptj.20110009.

[50] N. A. Bernstein, *The Coordination and Regulation of Movements*. Pergamon Press, 1967.

[51] N. A. Bernstein, *Bernstein’s construction of movement*. M. L. Latash Ed, Routledge, in press.

[52] D. J. Berger and A. d’Avella, “Effective force control by muscle synergies,” *Front Comput Neurosci*, vol. 8, Apr. 2014, doi: 10.3389/fncom.2014.00046.

[53] F. Lacquaniti and J. Soechting, “Coordination of arm and wrist motion during a reaching task,” *J Neurosci*, vol. 2, no. 4, pp. 399–408, Apr. 1982, doi: 10.1523/JNEUROSCI.02-04-00399.1982.

[54] T. Flash and N. Hogan, “The coordination of arm movements: an experimentally confirmed mathematical model,” *J. Neurosci.*, vol. 5, no. 7, pp. 1688–1703, Jul. 1985, doi: 10.1523/JNEUROSCI.05-07-01688.1985.

[55] B. Prilutsky, D. Ashley, L. VanHiel, L. Harley, J. Tidwell, and D. Backus, “Motor Control and Motor Redundancy in the Upper Extremity: Implications for Neurorehabilitation,” *Topics in Spinal Cord Injury Rehabilitation*, vol. 17, no. 1, pp. 7–15, Jul. 2011, doi: 10.1310/sci1701-07.

[56] Y. P. Ivanenko, G. Cappellini, N. Dominici, R. E. Poppele, and F. Lacquaniti, “Coordination of Locomotion with Voluntary Movements in Humans,” *J Neurosci*, vol. 25, no. 31, pp. 7238–7253, Aug. 2005, doi: 10.1523/JNEUROSCI.1327-05.2005.

[57] S. F. Giszter, “MOTOR PRIMITIVES - New Data and Future Questions,” Curr Opin Neurobiol, vol. 33, pp. 156–165, Aug. 2015, doi: 10.1016/j.conb.2015.04.004.

[58] M. P, “Spatial control of arm movements.,” Exp Brain Res, vol. 42, no. 2, pp. 223–227, Jan. 1981, doi: 10.1007/bf00236911.

[59] F. Lacquaniti, C. Terzuolo, and P. Viviani, “The law relating the kinematic and figural aspects of drawing movements,” *Acta Psychologica*, vol. 54, no. 1, pp. 115–130, Oct. 1983, doi: 10.1016/0001-6918(83)90027-6.

[60] P. M. Fitts, “The information capacity of the human motor system in controlling the amplitude of movement,” Journal of Experimental Psychology, vol. 47, no. 6, pp. 381–391, 1954, doi: 10.1037/h0055392.

[61] M. J. E. Richardson and T. Flash, “Comparing Smooth Arm Movements with the Two-Thirds Power Law and the Related Segmented-Control Hypothesis*,” J. Neurosci.*, vol. 22, no. 18, pp. 8201–8211, Sep. 2002, doi: 10.1523/JNEUROSCI.22-18-08201.2002.

[62] D. A. Winter, Biomechanics and motor control of human movement, 4th ed. Hoboken, N.J: Wiley, 2009.

[63] C. G. Atkeson and J. M. Hollerbach, “Kinematic features of unrestrained vertical arm movements,” *J. Neurosci.*, vol. 5, no. 9, pp. 2318–2330, Sep. 1985, doi: 10.1523/JNEUROSCI.05-09-02318.1985.

[64] “Reaction time - Human Homo sapiens - BNID 110799.” https://bionumbers.hms.harvard.edu/bionumber.aspx?s=n&v=2&id=110799 (accessed Jul. 07, 2020).

[65] S. Mazzoleni, M. Coscia, G. Rossi, S. Aliboni, F. Posteraro, and M.C. Carrozza, “Effects of upper limb robot-mediated therapy on paretic upper limb in chronic hemiparetic subjects: a biomechanical and EEG-based approach for functional assessment,” *11th International Conference on Rehabilitation Robotics*, Kyoto, Japan, June 23-26, 2009.

[66] J. Roh, W.Z. Rymer, and R.F. Beer, "Evidence for altered upper extremity muscle synergies in chronic stroke survivors with mild and moderate impairment," *Frontiers in Human Neuroscience*, vol. 9, no. 6, Feb. 2011.

[67] S. Solnik, P. DeVita, P. Rider, B. Long, and T. Hortobágyi, "Teager–Kaiser Operator improves the accuracy of EMG onset detection independent of signal-to-noise ratio," *Acta Bioeng Biomech,* vol. 10, no. 2, pp. 65–68, 2008.

[68] G. Pfurtscheller and F. H. Lopes Da Silva, "EEG Event-Related Desynchronization (ERD) and Event-Related Synchronization (ERS)," in *Niedermeyer's Electroencephalography: Basic Principles, Clinical Applications, and Related Fields,* 6th ed., 2010, pp. 935–948.

[69] William Rose, Electromyogram analysis, https://www1.udel.edu/biology/rosewc/kaap686/notes/EMG%20analysis.pdf (accessed Jun. 27, 2020)

[70] A. Delorme and S. Makeig, "EEGLAB: an open source toolbox for analysis of single-trial EEG dynamics including independent component analysis," *J. Neurosci. Methods*, vol. 134, no. 1, pp. 9–21, Mar. 2004, doi: 10.1016/j.jneumeth.2003.10.009.

[71] A. Farajidavar, J. M. Block, and M. Ghovanloo, "A comprehensive method for magnetic sensor calibration: A precise system for 3-D tracking of the tongue movements," *in 2012 Annual International Conference of the IEEE Engineering in Medicine and Biology Society*, Aug. 2012, pp. 1153–1156, doi: 10.1109/EMBC.2012.6346140.

[72] A. Ayala-Acevedo and M. Ghovanloo, "Smartphone-Compatible Robust Classification Algorithm for the Tongue Drive System," *Proc. IEEE Biomedical Circuits and Systems Conf.*, Lausanne, 2014, pp. 161-164.

[73] C. Chang and C. Lin, "LIBSVM: A library for Support Vector Machines," *ACM Transactions on Intelligent System and Technology (TST),* vol. 2, no. 27, Apr. 2011.

[74] F. Chu, R. Xu, Z. Zhang, P.A. Vela, and M. Ghovanloo, "The Helping Hand: An Assistive Manipulation Framework Using Augmented Reality and Tongue-Drive Interfaces," *2018 40th Annual International Conference of the IEEE Engineering in Medicine and Biology Society (EMBC),* Honolulu, HI, USA, pp. 2158-2161, July 18-21, 2018.